Monthly Notices
of the
ROYAL ASTRONOMICAL SOCIETY

Mon. Not. R. Astron. Soc. **402,** 1027–1048 (2010) doi:10.1111/j.1365-2966.2009.15938.x

An analysis of the timing irregularities for 366 pulsars

G. Hobbs,[1⋆] A. G. Lyne[2] and M. Kramer[2]

[1]*Australia Telescope National Facility, CSIRO, PO Box 76, Epping NSW 1710, Australia*
[2]*University of Manchester, Jodrell Bank Observatory, Macclesfield, Cheshire SK11 9DL*

Accepted 2009 October 23. Received 2009 October 11; in original form 2009 July 22

ABSTRACT

We provide an analysis of timing irregularities observed for 366 pulsars. Observations were obtained using the 76-m Lovell radio telescope at the Jodrell Bank Observatory over the past 36 years. These data sets have allowed us to carry out the first large-scale analysis of pulsar timing noise over time-scales of >10 yr, with multiple observing frequencies and for a large sample of pulsars. Our sample includes both normal and recycled pulsars. The timing residuals for the pulsars with the smallest characteristic ages are shown to be dominated by the recovery from glitch events, whereas the timing irregularities seen for older pulsars are quasi-periodic. We emphasize that previous models that explained timing residuals as a low-frequency noise process are not consistent with observation.

Key words: pulsars: general.

1 INTRODUCTION

The Jodrell Bank data archive of pulsar observations contains over 6000 years of pulsar rotational history. The pulsar timing method (for a general overview, see Manchester & Taylor 1977; Lyne & Smith 2004 or Lorimer & Kramer 2005; details are provided in Edwards, Hobbs & Manchester 2006) allows the observed pulse times of arrival (TOAs) to be compared with a model of the pulsar's astrometric, orbital and rotational parameters. The differences between the predicted arrival times and the actual arrival times are known as the pulsar 'timing residuals'. For a perfect model, the timing residuals would be dominated by measurement errors and have a 'white' spectrum. Any features observed in the timing residuals indicate the presence of unmodelled effects which may include calibration errors, orbital companions or spin-down irregularities. There are two main types of irregularity, namely 'glitches' which are sudden increases in rotation rate followed by a period of relaxation and 'timing noise' which consists of low-frequency structures.

A more complete understanding of pulsar timing noise will lead to many important results. For instance, explaining the cause of timing noise and glitches may also allow us to relate these phenomena and hence provide an insight into the interior structure of neutron stars. Pulsar timing array projects are being developed around the world with the aim of detecting gravitational waves by looking for irregularities in the timing of millisecond pulsars (see e.g. Hobbs 2005 and references therein). A stochastic background formed by coalescing supermassive binary black hole systems will induce signatures in the timing residuals with amplitudes of approximately 100 ns. If the intrinsic timing noise for millisecond pulsars is at a higher level, then it becomes more difficult to extract the gravitational wave signal from the observations.

In this paper, we study the timing noise in the residuals of 366 pulsars that have been regularly observed over the past 10 to 36 years. The basic observational parameters for the pulsars in our sample were provided by Hobbs et al. (2004, hereafter H04). These timing ephemerides included the pulsar positions, rotational frequencies and their first two derivatives, dispersion measures (DMs) and their derivatives and proper motions. The proper motions were subsequently updated with more recent observations, combined with other measurements of pulsar proper motions available from the literature and analysed by Hobbs et al. (2005). This work allowed us to present a new velocity distribution for the pulsar population.

In order to obtain the precise spin and astrometric parameters presented in H04, it was necessary to remove the low-frequency timing noise. This pre-whitening procedure was undertaken using a simple high-pass filter where harmonically related sinusoids were fitted to the residuals and the lowest frequency waves subtracted. The low-frequency noise was not subsequently studied in the previous papers. In this paper, we address the properties of this timing noise.

Low-frequency structures previously observed in pulsar data sets have been explained by random processes (e.g. Cordes & Helfand 1980; Lyne 1999), unmodelled planetary companions (e.g. Cordes 1993) or free-precession (e.g. Stairs, Lyne & Shemar 2000). However, the physical phenomenon underlying most of the timing noise still has not been explained. Much of the basic theoretical work was described by Boynton et al. (1972) who analysed the arrival times for the Crab pulsar over a 2-yr period. In their paper, an attempt was made to describe the timing noise as either phase, frequency or slowing-down noise corresponding to random walks in these parameters. Later, Cordes & Helfand (1980) found that out of a sample

⋆E-mail: george.hobbs@csiro.au

of 11 pulsars, seven showed timing noise consistent with frequency noise, two from slowing-down noise and two from phase noise. They concluded that (1) timing noise is widespread in pulsars, (2) it is correlated with period derivative and weakly with period and (3) it is not correlated with height above the Galactic plane, luminosity or with pulse shape changes. However, the data sets used were small in number, short and small-scale pulse shape variations would have been undetectable. The assumption that timing noise is a red-noise process has continued to date. However, Cordes & Downs (1985) showed that the idealized, random walk model was too simple. They developed a more detailed model where discrete 'micro-jumps' in one or more of the timing parameters were superimposed on the random walk process. D'Alessandro et al. (1995) analysed the timing residuals for 45 pulsars with data spanning up to 7 years. They observed very weak timing noise for 19 of their pulsars, for seven the activity was attributed to random walk processes comprising a large number of events in one of the rotation variables, a further seven were explained as resolved jumps in ν, the pulse frequency, and $\dot{\nu}$, its derivative, seven more as resolved jumps on a low-level background and for the remaining five the timing noise could not be explained as a pure random walk process or resolved jumps.

Timing noise analyses with large samples of pulsars have been limited by the relatively short data spans studied. Long data spans have been analysed in a few papers, but for only a small number of pulsars. For instance, Baykal et al. (1999) analysed four pulsars timed for 14 yr. Shabanova (1995) observed PSR B0329+54 for 16 yr, Stairs et al. (2000) reported on 13 yr of PSR B1828−11 observations and Shabanova, Lyne & Urama (2001) analysed PSR B1642−03 over a 30 yr data span. More recently, the millisecond pulsar PSR J1713+0747 was observed for 12 yr (Splaver et al. 2005) and the young pulsar PSR B1509−58 for 21 yr (Livingstone et al. 2005). Most of the analysis has concentrated on obtaining high-quality spectral estimates of the timing residuals or fitting a simple model to the timing residuals of a single pulsar. We note that our sample is ∼20 times larger than the previous large study of pulsar timing noise (D'Alessandro et al. 1995) in terms of the number of years of rotational history studied.

Glitches are thought to represent a sudden unpinning of superfluid vortices in the interior of the neutron star (Lyne, Shemar & Graham-Smith 2000). The relationship between glitches and timing noise is not understood although Janssen & Stappers (2006) showed that it is possible to model the timing noise in PSR B1951+32 as multiple small glitches. Glitches are discrete events that occur more commonly for young pulsars[1] (although for two pulsars with similar rotational parameters, one may glitch frequently while the other may never have been observed to glitch) and have a wide range of sizes with fractional frequency increases between 10^{-9} and 10^{-5} (e.g. Lyne et al. 2000; Hobbs et al. 2002). No model currently predicts the time between glitches or the size of any given event although pulsars with large glitches tend to show larger intervals between glitches (Lyne et al. 2000). Melatos, Peralta & Wyithe (2008) recently showed that, for most pulsars in their sample, the waiting time between glitch events followed an exponential distribution. This distribution was subsequently modelled by Warszawski & Melatos (2008) using a cellular automaton model of pulsar glitches. However, it is still not clear whether the glitch and timing noise phenomena are related.

In this paper, we describe the observing system and present the measured timing residuals (Section 2), rule out some models of timing noise (Section 3.1) and highlight various properties of the timing noise (Section 3.2).

2 RESULTS

The timing solutions for the pulsars in our sample have been updated since H04 with more recent data from the Jodrell Bank Observatory. The timing solutions were obtained using standard pulsar timing techniques as described in H04. In brief, the majority of the observations were obtained from the 76-m Lovell radio telescope. The earliest TOAs for 18 pulsars were obtained from observations using the NASA Deep Space Network (Downs & Reichley 1983; Downs & Krause-Polstorff 1986). Observations using the Lovell telescope were carried out predominately at frequencies close to 408, 610, 910, 1410 and 1630 MHz with a few early observations at 235 and 325 MHz. The last observations used in our data set were obtained around MJD 53500. The signals were combined to produce, for every observation, a total intensity profile. TOAs were subsequently determined by convolving, in the time domain, the profile with a template corresponding to the observing frequency. The pulsar timing residuals described in this paper were obtained by fitting a timing model to the TOAs using the TEMPO2 pulsar timing software (Hobbs, Edwards & Manchester 2006).

For those pulsars in which the residuals are dominated by large glitches, it is difficult to obtain phase coherent timing solutions across many years of observation. For example, for PSR B1800−21 we have data spanning from the year 1985 to the present. However, for this analysis we can only use data between the years 1991 and 1997. We have a similarly short data span for PSR B1727−33. Although PSRs B0531+21, B1758−23 and B1757−24 have been regularly observed, we cannot obtain a useful data set for the analysis described in this paper. These pulsars are therefore not included in our sample.

In Table 1, we present the basic parameters for our sample of pulsars. In column order, we first provide the pulsar's J2000 and B1950 names, spin-frequency, ν, frequency derivative, $\dot{\nu}$, and frequency second derivative, $\ddot{\nu}$. The following three columns give the epoch of the centre of the data span, the number of observations and the time-span of the observations. We then provide various measures characterizing the amount of timing noise for each data set. We present σ_1, the unweighted rms of the residuals after fitting for ν and $\dot{\nu}$, σ_2, the unweighted rms of the residuals after removal of ν and its first two derivatives and σ_3, the rms after whitening the data set by fitting, and removing, harmonically related sinusoids (as described in H04). The last two columns contain two stability measures (Δ_8 and σ_z) that are discussed in Section 3.2.1.

A period–period-derivative diagram[2] for the pulsars in our sample is shown in Fig. 1 to indicate the range of pulsar parameters included in our sample. The diagram includes dotted lines representing various characteristic ages $\tau_c = P/(2\dot{P})$ and dashed lines for representative surface magnetic field strengths $B_s = 3.2 \times 10^{19}\sqrt{P\dot{P}}$ G. A histogram indicating the time-spans of our observations is shown in Fig. 2. The mean and median time-spans are 18.5 and 18.3 yr, respectively. For the recycled pulsars, the unweighted rms of the

[1] We use the terms 'young' and 'old' throughout referring to a pulsar's characteristic age which is only an approximation of the pulsar's true age.

[2] Note that we have attempted to be consistent in our use of pulse frequency and its derivatives. However, in order to make a direct comparison with earlier publications we sometimes use the pulse period and its derivatives where $P = 1/\nu$, $\dot{P} = -\dot{\nu}/\nu^2$.

Table 1. Basic parameters for the pulsars in our sample. σ_1 is the rms residual after removing a quadratic term, σ_2 the rms value after removing a cubic term and σ_3 the value after whitening the data.

PSR J	PSR B	ν (s^{-1})	$\dot{\nu}$ ($10^{-15}\,s^{-2}$)	$\ddot{\nu}$ ($10^{-24}\,s^{-3}$)	Epoch (MJD)	N	T_s (yr)	σ_1 (ms)	σ_2 (ms)	σ_3 (ms)	Δ_8	$\log\sigma_z(10\,\mathrm{yr})$
J0014+4746	B0011+47	0.806	−0.367	0.00035(20)	49285.0	365	22.8	4.26	4.23	4.23	< −1.14	−10.91
J0034−0534	—	532.713	−1.409	−0.043(10)	51096.0	402	12.8	0.06	0.06	0.06	< −3.04	−12.44
J0034−0721	B0031−07	1.061	−0.459	0.00033(3)	47051.0	772	35.0	3.84	3.47	3.38	−1.44	−10.79
J0040+5716	B0037+56	0.894	−2.302	−0.00005(6)	50091.0	426	18.5	0.62	0.62	0.62	< −1.79	−11.65
J0048+3412	B0045+33	0.822	−1.589	−0.0003(3)	50083.0	201	18.4	2.17	2.15	2.15	< −1.21	−11.06
J0055+5117	B0052+51	0.473	−2.132	0.00092(5)	50092.0	417	18.5	1.51	1.08	1.08	< −1.63	−11.03
J0056+4756	B0053+47	2.118	−14.938	−0.0083(18)	50103.0	252	18.2	6.09	5.82	2.29	< −1.36	−10.24
J0102+6537	B0059+65	0.596	−2.113	−0.02862(17)	50091.0	339	18.5	65.23	2.66	1.37	< −1.34	−9.91
J0108+6608	B0105+65	0.779	−7.918	0.107(16)	50482.0	427	16.2	157.09	148.26	3.51	−0.16	−8.70
J0108+6905	B0105+68	0.934	−0.042	−0.0002(3)	50091.0	336	18.5	2.63	2.62	2.62	< −1.36	−11.21
J0108−1431	—	1.238	−0.118	−0.0030(18)	51251.0	332	12.1	4.49	4.47	4.47	< −1.45	−10.84
J0117+5914	B0114+58	9.858	−568.596	−2.91(3)	50083.0	314	18.4	165.07	25.71	0.34	−1.55	−9.21
J0134−2937	—	7.301	−4.178	−0.0004(5)	51251.0	298	12.1	0.19	0.19	0.19	< −2.59	−12.53
J0139+5814	B0136+57	3.670	−144.309	−0.065(10)	49706.0	684	20.6	56.33	52.63	0.20	−0.95	−9.27
J0141+6009	B0138+59	0.818	−0.261	0.00029(6)	49495.0	451	19.4	1.09	1.06	1.06	< −2.24	−11.51
J0147+5922	B0144+59	5.094	−6.661	0.0255(7)	50080.0	430	18.2	2.72	1.16	0.16	−2.56	−10.62
J0152−1637	B0149−16	1.201	−1.874	−0.00425(5)	48651.0	455	26.4	5.79	1.39	0.59	< −2.07	−11.10
J0156+3949	B0153+39	0.552	−0.046	−0.0001(13)	50104.0	81	18.1	9.88	9.88	9.88	−0.31	−10.46
J0157+6212	B0154+61	0.425	−34.160	−0.0093(8)	50126.0	463	18.3	26.74	20.09	2.18	−1.49	−9.73
J0215+6218	—	1.822	−2.198	−0.0095(8)	51788.0	327	10.5	1.46	0.98	0.43	−2.29	−10.62
J0218+4232	—	430.461	−14.340	−0.007(8)	51268.0	387	11.9	0.05	0.05	0.05	< −3.26	−13.04
J0231+7026	B0226+70	0.682	−1.445	0.00026(13)	50088.0	305	18.5	1.83	1.81	1.81	< −1.36	−10.98
J0304+1932	B0301+19	0.721	−0.673	−0.00274(7)	49141.0	498	23.7	4.26	1.76	1.00	< −1.39	−10.54
J0323+3944	B0320+39	0.330	−0.069	0.00004(4)	49229.0	520	23.2	2.25	2.24	2.24	< −1.71	−11.35
J0332+5434	B0329+54	1.400	−4.012	0.00092(7)	46775.0	1170	36.5	7.46	6.76	0.46	−1.86	−10.38
J0335+4555	B0331+45	3.715	−0.101	0.00014(12)	50081.0	483	18.4	0.33	0.33	0.33	< −2.33	−12.19
J0343+5312	B0339+53	0.517	−3.587	−0.00131(15)	49557.0	325	22.9	4.64	4.13	4.13	< −1.24	−10.42
J0357+5236	B0353+52	5.075	−12.277	0.0078(4)	50081.0	412	18.4	0.98	0.63	0.18	< −2.39	−10.79
J0406+6138	B0402+61	1.682	−15.773	0.0476(19)	50428.0	406	16.7	13.77	8.43	0.43	−1.57	−9.69
J0415+6954	B0410+69	2.559	−0.502	0.00142(11)	50092.0	375	18.5	0.51	0.41	0.36	< −2.17	−11.32
J0421−0345	—	0.463	−0.249	0.00110(15)	50847.0	226	13.3	1.27	1.13	1.13	< −1.71	−10.84
J0448−2749	—	2.220	−0.731	−0.0029(9)	51427.0	332	11.2	0.88	0.85	0.85	< −2.03	−11.43
J0450−1248	B0447−12	2.283	−0.535	−0.0010(3)	49751.0	527	20.2	1.68	1.64	1.64	< −2.00	−11.29
J0452−1759	B0450−18	1.822	−19.092	0.0137(5)	49295.0	576	22.9	8.21	5.15	0.29	−1.97	−10.16
J0454+5543	B0450+55	2.935	−20.441	−0.184(4)	50336.0	335	17.2	29.42	10.56	0.33	−1.70	−9.51
J0459−0210	—	0.883	−1.089	−0.0004(5)	51269.0	238	12.0	1.34	1.34	1.34	< −1.50	−11.53
J0502+4654	B0458+46	1.566	−13.690	0.01057(16)	49129.0	497	23.6	7.35	2.19	0.54	−1.98	−10.69
J0520−2553	—	4.138	−0.515	0.0026(12)	51657.0	181	10.2	0.42	0.41	0.41	< −1.98	−11.46
J0525+1115	B0523+11	2.821	−0.586	−0.000238(20)	48663.0	643	26.3	0.32	0.28	0.26	< −2.46	−11.78
J0528+2200	B0525+21	0.267	−2.854	0.00082(4)	46909.0	954	35.8	20.34	15.25	1.39	< −1.38	−10.01
J0538+2817	—	6.985	−179.088	−0.6951(12)	51821.0	353	10.1	21.28	0.34	0.18	−1.91	−9.48
J0543+2329	B0540+23	4.065	−254.898	0.2173(15)	49294.0	691	22.9	46.67	7.89	0.16	−2.09	−10.03
J0612+3721	B0609+37	3.356	−0.670	−0.0125(3)	50092.0	456	18.5	2.07	0.80	0.35	< −2.38	−10.81
J0613−0200	—	326.601	−1.019	0.009(4)	51240.0	656	12.1	0.04	0.04	0.04	< −3.47	−12.89
J0614+2229	B0611+22	2.985	−529.522	9.51(8)	50164.0	973	18.1	1735.68	514.15	1.82	−0.14	−7.97
J0621+1002	—	34.657	−0.057	0.0019(3)	51145.0	685	10.8	0.03	0.03	0.03	−3.41	−12.79
J0624−0424	B0621−04	0.962	−0.769	0.00001(10)	50302.0	459	17.4	0.87	0.87	0.87	< −1.77	−11.63
J0629+2415	B0626+24	2.098	−8.785	0.0049(8)	49846.0	541	19.7	5.75	5.53	0.41	−1.96	−10.30
J0630−2834	B0628−28	0.804	−4.601	−0.0175(7)	47013.0	807	35.2	131.89	91.99	1.52	−1.84	−9.71
J0653+8051	B0643+80	0.823	−2.576	0.00069(4)	49141.0	283	23.7	1.23	0.83	0.70	< −1.84	−11.01
J0659+1414	B0656+14	2.598	−371.288	0.7636(19)	49721.0	772	16.1	120.42	7.27	1.49	−1.26	−9.09
J0700+6418	B0655+64	5.111	−0.018	0.00019(13)	49138.0	402	23.7	0.64	0.64	0.64	< −2.06	−11.48
J0725−1635	—	2.357	−0.515	−0.0018(4)	50884.0	277	13.3	0.57	0.54	0.54	< −2.00	−11.24
J0729−1836	B0727−18	1.960	−72.832	0.245(7)	50126.0	635	18.3	76.04	40.15	0.55	−0.55	−9.05
J0742−2822	B0740−28	5.997	−604.876	−0.61(5)	49696.0	1009	20.6	165.35	145.16	0.40	−0.84	−8.92

Table 1 – *continued*

PSR J	PSR B	ν (s^{-1})	$\dot{\nu}$ ($10^{-15}\,s^{-2}$)	$\ddot{\nu}$ ($10^{-24}\,s^{-3}$)	Epoch (MJD)	N	T_s (yr)	σ_1 (ms)	σ_2 (ms)	σ_3 (ms)	Δ_8	$\log\sigma_z(10\,\mathrm{yr})$
J0751+1807	—	287.458	−0.643	−0.002(4)	51389.0	531	11.3	0.04	0.04	0.04	< −3.67	−13.55
J0754+3231	B0751+32	0.693	−0.519	−0.00081(6)	49763.0	492	20.3	1.54	1.28	1.21	< −1.79	−11.04
J0814+7429	B0809+74	0.774	−0.101	0.00014(5)	49369.0	474	22.4	1.07	1.06	1.06	< −1.59	−11.47
J0820−1350	B0818−13	0.808	−1.373	0.000028(19)	49299.0	631	22.7	0.55	0.55	0.26	< −2.24	−11.62
J0823+0159	B0820+02	1.156	−0.140	−0.00075(5)	49144.0	573	23.7	1.10	0.88	0.84	−2.00	−11.08
J0826+2637	B0823+26	1.884	−6.069	0.0240(12)	46857.0	979	36.1	110.89	90.82	0.29	−1.63	−9.49
J0828−3417	B0826−34	0.541	−0.292	−0.0035(5)	48508.0	146	25.9	19.16	16.03	14.04	<0.16	−9.88
J0837+0610	B0834+06	0.785	−4.191	0.000096(11)	49138.0	604	23.7	0.36	0.34	0.34	< −1.91	−11.73
J0846−3533	B0844−35	0.896	−1.285	0.00107(13)	49145.0	119	23.7	1.95	1.52	1.52	< −0.95	−10.98
J0849+8028	B0841+80	0.624	−0.174	0.00005(74)	50419.0	90	16.6	4.80	4.79	4.79	< −0.42	−10.70
J0855−3331	B0853−33	0.789	−3.934	0.00059(15)	49735.5	435	17.2	1.63	1.60	1.60	< −1.66	−11.07
J0908−1739	B0906−17	2.490	−4.151	0.00165(5)	49140.0	639	23.7	0.75	0.43	0.29	−2.49	−11.23
J0921+6254	B0917+63	0.638	−1.468	0.00018(12)	49687.0	156	16.3	0.86	0.85	0.85	< −1.58	−11.18
J0922+0638	B0919+06	2.322	−73.982	0.1385(12)	48518.0	766	27.0	99.33	22.52	0.35	−1.07	−9.36
J0943+1631	B0940+16	0.920	−0.077	0.00008(17)	49143.0	443	23.7	4.04	4.04	4.04	< −1.03	−11.24
J0944−1354	B0942−13	1.754	−0.139	−0.00027(5)	49764.0	533	20.3	0.41	0.40	0.40	< −2.62	−11.83
J0946+0951	B0943+10	0.911	−2.902	−0.0377(8)	49352.0	117	22.3	47.86	10.29	10.29	−0.28	−9.79
J0953+0755	B0950+08	3.952	−3.588	−0.0048(3)	46777.0	953	36.5	11.22	9.53	0.12	−2.31	−10.53
J1012+5307	—	190.268	−0.620	0.0031(12)	51331.0	521	11.6	0.02	0.02	0.02	< −3.91	−13.30
J1012−2337	B1010−23	0.397	−0.139	0.00012(12)	49127.0	137	23.6	4.66	4.56	4.56	<0.25	−10.70
J1018−1642	B1016−16	0.554	−0.535	0.00006(18)	50093.0	243	18.5	2.79	2.78	2.78	< −1.12	−11.78
J1022+1001	—	60.779	−0.160	0.0014(4)	51638.0	625	11.2	0.02	0.02	0.02	< −3.99	−13.56
J1024−0719	—	193.716	−0.695	0.007(6)	51422.0	366	11.0	0.06	0.06	0.06	< −3.32	−13.22
J1034−3224	—	0.869	−0.174	−0.0005(6)	51123.0	225	12.9	1.83	1.82	1.82	< −1.37	−11.89
J1041−1942	B1039−19	0.721	−0.492	−0.0000009(500)	49143.0	477	23.7	1.31	1.30	1.30	< −1.78	−11.63
J1047−3032	—	3.027	−0.559	−0.004(3)	51445.0	264	11.1	1.84	1.84	1.84	< −1.81	−11.24
J1115+5030	B1112+50	0.604	−0.909	−0.00006(5)	49753.0	491	20.2	1.28	1.28	1.28	< −1.90	−11.60
J1136+1551	B1133+16	0.842	−2.646	0.00125(6)	46407.0	900	36.4	15.22	13.76	0.24	< −2.07	−10.92
J1141−3107	—	1.857	−6.880	−0.61(3)	51271.0	179	12.1	71.87	37.79	2.94	−0.30	−8.91
J1141−3322	—	6.862	−10.921	−0.291(14)	51446.0	328	11.1	6.64	4.22	0.51	< −2.15	−9.88
J1238+21	B1238+21	0.894	−1.155	−0.0010(16)	51822.0	82	10.1	1.81	1.80	1.80	< −1.35	−11.23
J1239+2453	B1237+25	0.723	−0.502	−0.000305(9)	46942.0	1026	35.6	3.15	2.12	0.57	< −2.11	−11.17
J1257−1027	B1254−10	1.620	−0.952	−0.00009(16)	49348.2	475	18.4	1.12	1.12	1.09	< −1.96	−11.46
J1300+1240	B1257+12	160.810	−2.957	−0.002(3)	50788.0	360	14.5	0.08	0.07	0.07	< −3.09	−13.10
J1311−1228	B1309−12	2.235	−0.753	−0.00141(12)	50094.0	433	18.5	0.65	0.56	0.49	< −2.11	−11.16
J1321+8323	B1322+83	1.492	−1.262	−0.0056(3)	49282.0	289	22.8	3.97	2.30	2.30	< −1.41	−10.58
J1332−3032	—	1.537	−1.322	0.017(9)	51447.0	192	11.1	9.62	9.52	9.52	< −0.96	−10.46
J1455−3330	—	125.200	−0.381	−0.008(4)	51190.0	269	12.4	0.07	0.07	0.07	< −2.94	−12.46
J1509+5531	B1508+55	1.352	−9.144	0.0819(15)	49294.0	471	22.9	63.60	22.20	0.52	−1.52	−9.87
J1518+4904	—	24.429	−0.016	0.0002(5)	51619.0	309	10.0	0.03	0.03	0.03	< −3.48	−13.21
J1532+2745	B1530+27	0.889	−0.616	−0.0024(3)	50096.0	414	18.5	3.37	3.03	1.62	< −1.64	−10.55
J1537+1155	B1534+12	26.382	−1.686	0.00008(30)	50300.0	400	13.8	0.04	0.04	0.04	< −3.14	−12.88
J1543+0929	B1541+09	1.336	−0.772	−0.0093(4)	49141.0	452	23.7	10.61	6.46	3.27	< −1.28	−10.03
J1543−0620	B1540−06	1.410	−1.749	0.0130(3)	49839.0	503	19.7	7.06	3.02	0.36	−1.36	−10.36
J1555−2341	B1552−23	1.878	−2.447	−0.0280(4)	50301.0	346	17.3	6.42	1.40	0.88	< −1.90	−10.23
J1555−3134	B1552−31	1.930	−0.232	−0.00018(19)	50299.0	289	17.3	0.69	0.69	0.69	< −1.92	−11.58
J1603−2531	—	3.533	−19.875	−0.068(12)	51121.0	192	12.8	9.21	8.47	0.15	−1.72	−9.85
J1603−2712	B1600−27	1.285	−4.968	−0.0025(3)	50302.0	199	17.3	1.61	1.36	0.67	< −1.91	−10.72
J1607−0032	B1604−00	2.371	−1.720	−0.002015(10)	47386.0	729	33.2	3.53	0.47	0.44	< −2.38	−11.30
J1610−1322	B1607−13	0.982	−0.222	−0.0003(6)	50094.0	213	18.5	4.77	4.75	4.75	< −1.02	−10.81
J1614+0737	B1612+07	0.829	−1.620	−0.0007(3)	49897.0	160	15.1	1.19	1.12	1.12	< −1.78	−11.24
J1615−2940	B1612−29	0.404	−0.258	0.00012(17)	49026.0	99	23.1	4.91	4.89	4.89	−0.18	−10.58
J1623−0908	B1620−09	0.783	−1.584	0.00027(3)	49142.0	394	23.7	0.85	0.75	0.75	< −1.08	−11.30
J1623−2631	B1620−26	90.287	−2.953	18.346(11)	50292.0	768	17.5	103.55	3.06	0.15	−1.35	−9.22
J1635+2418	B1633+24	2.039	−0.496	0.00070(20)	49130.0	149	23.6	1.23	1.18	1.18	< −1.28	−11.23

Table 1 – *continued*

PSR J	PSR B	ν (s^{-1})	$\dot{\nu}$ ($10^{-15}\,s^{-2}$)	$\ddot{\nu}$ ($10^{-24}\,s^{-3}$)	Epoch (MJD)	N	T_s (yr)	σ_1 (ms)	σ_2 (ms)	σ_3 (ms)	Δ_8	$\log\sigma_z(10\,\mathrm{yr})$
J1643−1224	—	216.373	−0.865	−0.0043(19)	51251.0	433	12.0	0.03	0.03	0.03	< −3.30	−13.10
J1645−0317	B1642−03	2.579	−11.846	0.0067(6)	46930.0	957	35.7	21.63	20.68	0.22	−0.99	−9.66
J1648−3256	—	1.390	−6.815	0.004(3)	51276.0	149	12.0	4.54	4.50	0.76	−1.39	−10.26
J1650−1654	—	0.572	−1.046	−0.0027(8)	51272.0	172	12.1	3.07	2.95	2.95	−1.06	−10.72
J1651−1709	B1648−17	1.027	−3.205	0.0007(4)	50430.0	168	16.7	1.56	1.53	1.31	< −1.30	−11.06
J1652−2404	B1649−23	0.587	−1.088	−0.00155(5)	49132.0	348	23.6	3.36	1.70	1.60	< −1.61	−10.91
J1654−2713	—	1.263	−0.268	0.002(3)	51414.0	154	11.1	2.39	2.38	2.38	< −1.19	−11.04
J1659−1305	B1657−13	1.560	−1.503	0.0309(7)	50094.0	147	18.5	10.86	2.66	2.66	< −1.02	−10.12
J1700−3312	—	0.736	−2.555	−0.0163(6)	51276.0	250	12.0	3.96	1.87	1.41	< −1.42	−10.28
J1703−1846	B1700−18	1.243	−2.676	0.00003(12)	50314.0	209	17.3	0.56	0.56	0.56	< −1.98	−12.02
J1703−3241	B1700−32	0.825	−0.449	0.00122(9)	50427.0	159	16.6	0.78	0.51	0.51	< −1.58	−11.08
J1705−1906	B1702−19	3.345	−46.284	−0.0009(6)	50497.0	410	16.3	1.28	1.24	0.25	< −2.36	−11.11
J1705−3423	—	3.915	−16.484	0.085(6)	51256.0	152	11.9	4.72	2.85	1.01	−1.55	−9.96
J1708−3426	—	1.445	−8.775	−0.0100(15)	51276.0	124	12.0	2.42	2.05	2.05	< −1.12	−10.62
J1709−1640	B1706−16	1.531	−14.783	0.3704(12)	47389.0	498	33.2	948.18	63.69	0.43	−1.14	−9.07
J1711−1509	B1709−15	1.151	−1.461	0.0067(3)	50094.0	197	18.5	3.78	1.72	0.67	< −1.71	−10.65
J1713+0747	—	218.812	−0.409	0.0019(13)	51318.0	345	11.5	0.01	0.01	0.01	−3.94	−13.51
J1717−3425	B1714−34	1.524	−22.761	0.022(8)	50673.0	139	15.2	17.88	17.35	0.82	−0.74	−9.51
J1720−0212	B1718−02	2.093	−0.363	−0.0001(6)	49853.0	320	19.8	3.44	3.44	3.44	< −1.53	−12.20
J1720−1633	B1717−16	0.639	−2.366	−0.00002(72)	50084.0	214	18.4	8.95	8.95	1.57	−1.20	−10.06
J1720−2933	B1717−29	1.612	−1.938	−0.0142(3)	50290.0	164	17.2	3.88	0.87	0.69	< −1.58	−10.62
J1721−1936	B1718−19	0.996	−1.609	0.153(13)	50840.0	288	14.4	67.75	54.68	2.99	−0.83	−8.89
J1721−3532	B1718−35	3.566	−320.260	−0.07(6)	51505.0	139	10.7	20.82	20.24	0.90	−0.98	−10.71
J1722−3207	B1718−32	2.096	−2.838	−0.0010(7)	50495.0	180	16.3	1.72	1.70	0.16	−2.12	−10.84
J1728−0007	B1726−00	2.591	−7.535	−0.0167(7)	50513.0	152	16.1	2.88	1.28	0.93	< −1.64	−10.81
J1730−2304	—	123.110	−0.306	−0.0053(13)	51240.0	444	12.0	0.03	0.03	0.03	< −3.49	−12.73
J1730−3350	B1727−33	7.170	−4355.079	62.8(4)	51419.0	220	8.1	408.75	30.19	0.70	0.28	−7.21
J1732−1930	—	2.067	−0.776	−0.004(3)	51644.0	100	10.1	1.40	1.38	1.38	< −1.42	−11.03
J1733−2228	B1730−22	1.147	−0.056	−0.00006(8)	49140.0	395	23.7	1.40	1.40	1.40	< −1.27	−11.50
J1734−0212	B1732−02	1.191	−0.597	0.0026(8)	50117.0	127	18.3	3.53	3.36	3.36	< −0.88	−10.59
J1735−0724	B1732−07	2.385	−6.908	0.0019(4)	50312.0	342	17.3	1.22	1.18	0.25	−2.08	−10.85
J1738−3211	B1735−32	1.301	−1.346	0.00044(14)	50018.0	365	18.9	1.34	1.32	1.29	< −1.90	−11.37
J1739−2903	B1736−29	3.097	−75.578	0.127(4)	49872.0	394	19.7	28.59	12.75	0.85	−1.52	−9.54
J1739−3131	B1736−31	1.889	−66.269	0.78(5)	49884.0	244	18.1	326.94	174.40	0.90	−0.11	−8.49
J1740+1311	B1737+13	1.245	−2.250	0.01946(14)	48669.0	442	26.3	24.89	3.58	0.55	< −1.94	−10.30
J1741+2758	—	0.735	−0.994	−0.0007(15)	51750.0	104	10.4	2.48	2.34	2.34	< −1.21	−11.48
J1741−0840	B1738−08	0.489	−0.545	−0.00008(10)	50306.0	297	17.2	1.38	1.37	1.37	< −1.53	−11.42
J1743−0339	B1740−03	2.249	−7.873	0.41(4)	50199.0	139	16.6	111.71	76.44	1.71	−0.44	−8.72
J1743−1351	B1740−13	2.467	−2.910	−0.080(3)	50095.0	184	18.5	19.27	8.52	1.13	< −1.49	−9.88
J1743−3150	B1740−31	0.414	−20.716	−0.0185(7)	50674.0	284	15.3	17.60	8.73	2.76	< −1.22	−9.67
J1744−1134	—	245.426	−0.539	−0.0076(12)	51490.0	282	10.7	0.01	0.01	0.01	< −4.19	−12.95
J1745−3040	B1742−30	2.722	−79.021	−0.0629(18)	50311.0	393	17.3	10.69	4.96	0.18	−2.04	−10.01
J1748−1300	B1745−12	2.537	−7.808	−0.0347(7)	50315.0	289	17.3	5.91	1.86	0.26	−2.10	−10.34
J1748−2021	B1745−20	3.465	−4.803	0.059(8)	50677.0	362	15.3	14.84	13.67	13.67	< −0.75	−9.96
J1748−2444	—	2.258	−0.568	−0.0024(12)	50917.0	190	14.2	1.82	1.80	1.73	< −1.62	−11.02
J1749−3002	B1746−30	1.640	−21.163	−0.052(2)	50653.0	193	15.2	11.54	5.34	1.96	< −1.33	−9.93
J1750−3157	B1747−31	1.098	−0.237	0.0004(4)	50674.0	213	15.3	1.37	1.36	1.36	< −1.55	−11.45
J1750−3503	—	1.462	−0.079	0.031(16)	51426.0	131	11.2	15.89	15.65	15.65	< −0.62	−10.00
J1752−2806	B1749−28	1.778	−25.687	0.0087(10)	46889.0	655	35.8	67.62	63.41	0.44	−1.15	−9.45
J1753−2501	B1750−24	1.893	−50.565	−0.014(5)	49883.0	216	19.6	22.35	21.63	3.82	< −1.22	−9.78
J1754+5201	B1753+52	0.418	−0.274	−0.0003(3)	50095.0	296	18.5	5.08	5.06	5.06	< −0.97	−10.82
J1756−2435	B1753−24	1.491	−0.633	−0.00005(12)	49848.0	232	18.8	0.75	0.75	0.75	< −1.80	−11.67
J1757−2421	B1754−24	4.272	−235.755	0.283(3)	49121.0	397	22.8	92.18	29.55	0.76	−1.04	−9.55
J1759−2205	B1756−22	2.169	−51.171	−0.213(3)	50126.0	388	18.3	49.92	11.50	0.31	−1.73	−9.41
J1759−2922	—	1.741	−14.028	0.0017(9)	51256.0	133	11.9	0.96	0.95	0.95	< −1.46	−11.17

Table 1 – *continued*

PSR J	PSR B	ν (s^{-1})	$\dot{\nu}$ ($10^{-15}\,s^{-2}$)	$\ddot{\nu}$ ($10^{-24}\,s^{-3}$)	Epoch (MJD)	N	T_s (yr)	σ_1 (ms)	σ_2 (ms)	σ_3 (ms)	Δ_8	$\log\sigma_z(10\,\mathrm{yr})$
J1801−0357	B1758−03	1.085	−3.897	−0.032(3)	50084.0	201	18.4	22.82	16.73	0.67	< −1.36	−9.71
J1801−2920	B1758−29	0.924	−2.814	−0.0041(8)	51417.0	229	11.0	1.58	1.49	0.59	−1.81	−10.63
J1803−2137	B1800−21	7.484	−7511.371	224.89(3)	49527.0	352	6.7	2375.83	1.87	0.99	0.73	−6.74
J1803−2712	B1800−27	2.990	−0.153	0.0006(10)	50661.0	151	15.1	1.18	1.17	1.17	< −1.06	−11.19
J1804−0735	B1802−07	43.288	−0.875	0.0041(20)	50709.0	433	15.0	0.28	0.28	0.28	< −2.45	−12.05
J1804−2717	—	107.032	−0.468	−0.008(5)	51440.0	261	10.9	0.07	0.07	0.07	< −3.17	−12.45
J1805+0306	B1802+03	4.572	−20.892	0.0444(18)	50331.0	198	16.9	3.85	1.83	0.26	< −1.76	−10.48
J1806−1154	B1804−12	1.913	−5.157	0.0287(9)	51096.0	180	12.8	3.01	1.06	0.75	< −1.59	−10.50
J1807−0847	B1804−08	6.108	−1.074	−0.00326(10)	48671.0	456	26.3	1.13	0.54	0.09	< −3.00	−11.39
J1807−2715	B1804−27	1.208	−17.768	−0.0863(7)	50291.0	233	17.2	27.64	3.29	0.76	< −1.66	−9.57
J1808−0813	—	1.141	−1.616	0.0026(5)	51271.0	154	12.0	0.99	0.90	0.90	< −1.63	−10.88
J1808−2057	B1805−20	1.089	−20.243	0.0773(6)	49937.0	188	18.8	48.80	4.60	0.97	−0.92	−9.72
J1809−2109	B1806−21	1.424	−7.747	−0.0082(5)	49995.0	227	18.8	4.93	3.09	0.34	−1.91	−10.54
J1812+0226	B1810+02	1.260	−5.711	0.0009(3)	50336.0	244	17.1	1.32	1.28	1.28	< −1.59	−11.00
J1812−1718	B1809−173	0.830	−13.128	0.082(4)	49887.0	234	19.6	84.15	48.55	1.03	−1.20	−8.83
J1812−1733	B1809−176	1.858	−3.390	−0.0137(13)	50688.0	191	15.2	3.81	2.99	2.99	< −1.33	−10.42
J1813+4013	B1811+40	1.074	−2.939	0.01304(20)	50300.0	266	17.2	5.10	1.16	0.85	< −1.64	−10.50
J1816−1729	B1813−17	1.278	−11.873	−0.199(3)	49887.0	238	19.6	106.40	18.59	0.63	−1.46	−9.24
J1816−2650	B1813−26	1.687	−0.189	−0.00109(16)	49573.9	261	23.6	2.04	1.88	1.88	< −1.12	−11.18
J1818−1422	B1815−14	3.431	−23.995	−0.015(4)	49993.0	218	18.8	8.75	8.32	0.28	−1.61	−9.90
J1820−0427	B1818−04	1.672	−17.700	0.0277(7)	47020.0	690	35.1	93.58	45.77	0.66	−1.01	−9.19
J1820−1346	B1817−13	1.085	−5.294	0.0129(3)	50018.0	218	18.9	8.06	2.03	1.18	< −1.64	−10.26
J1820−1818	B1817−18	3.227	−0.975	0.0042(5)	50663.0	170	15.1	0.71	0.58	0.58	−1.69	−11.23
J1821+1715	B1821+17	0.732	−0.466	0.0006(15)	51819.0	112	10.2	2.41	2.39	2.39	< −1.08	−11.33
J1822+0705	—	0.734	−0.941	0.0013(7)	51748.0	102	10.6	1.24	1.15	1.15	< −1.36	−11.05
J1822−1400	B1820−14	4.656	−19.666	−0.101(6)	50042.0	208	18.8	16.84	10.36	0.86	−1.32	−9.79
J1822−2256	B1819−22	0.534	−0.385	0.00007(12)	49120.0	164	16.0	1.10	1.10	1.10	< −1.46	−11.44
J1823+0550	B1821+05	1.328	−0.400	−0.00156(6)	49844.0	365	19.8	1.02	0.60	0.36	< −2.13	−11.08
J1823−0154	—	1.316	−1.960	−0.0085(5)	51276.0	157	12.0	1.36	0.71	0.54	< −1.68	−10.51
J1823−1115	B1820−11	3.574	−17.612	−0.163(4)	49993.0	469	18.8	26.54	11.44	2.88	−1.63	−9.82
J1823−3021A	B1820−30A	183.823	−114.336	0.522(4)	50719.0	302	15.0	0.85	0.09	0.09	−2.95	−11.06
J1823−3021B	B1820−30B	2.641	−0.225	0.0031(5)	50700.0	303	14.9	0.79	0.72	0.61	< −2.00	−11.11
J1823−3106	B1820−31	3.520	−36.277	−0.134(5)	50315.0	238	17.3	17.68	8.26	0.20	−1.73	−9.67
J1824−1118	B1821−11	2.295	−18.716	0.059(5)	49874.0	233	19.6	26.36	20.37	0.86	−1.35	−9.57
J1824−1945	B1821−19	5.282	−145.939	−0.152(19)	50101.0	351	18.2	37.37	33.81	0.24	−1.19	−9.31
J1824−2452	B1821−24	327.406	−173.519	0.047(7)	50238.0	163	17.4	0.13	0.11	0.09	< −2.56	−12.06
J1825+0004	B1822+00	1.284	−1.445	−0.0076(5)	50336.0	240	17.1	3.29	2.21	0.61	< −1.54	−10.46
J1825−0935	B1822−09	1.300	−88.369	1.541(16)	49831.0	506	19.7	855.97	172.69	1.21	−0.44	−8.15
J1825−1446	B1822−14	3.582	−290.947	0.190(4)	49862.0	234	19.5	41.52	9.05	0.77	−1.38	−9.62
J1826−1131	B1823−11	0.478	−1.121	0.00454(13)	49867.0	340	19.7	7.12	3.17	2.36	< −1.42	−10.55
J1826−1334	B1823−13	9.856	−7293.991	138.2(4)	50639.9	591	11.8	2267.62	123.04	0.58	0.37	−7.28
J1827−0958	B1824−10	4.069	−16.597	−0.0399(15)	49883.0	253	19.6	7.28	3.63	1.73	< −1.60	−10.18
J1829−1751	B1826−17	3.256	−58.852	0.048(3)	50101.0	363	18.2	10.66	7.31	0.44	−0.68	−9.65
J1830−1059	B1828−11	2.469	−365.843	0.865(3)	50031.0	755	18.7	217.18	16.82	0.47	−0.80	−8.68
J1832−0827	B1829−08	1.545	−152.462	−0.011(4)	49868.0	359	19.7	40.85	28.31	0.41	−1.63	−9.82
J1832−1021	B1829−10	3.027	−38.493	0.247(3)	49883.0	372	19.6	52.02	10.37	0.52	−1.57	−9.55
J1833−0338	B1831−03	1.456	−88.139	0.104(5)	50123.0	499	18.3	45.86	30.84	0.50	−0.66	−9.18
J1833−0827	B1830−08	11.725	−1260.890	−1.357(9)	50740.0	351	14.7	37.77	3.72	0.24	−1.49	−9.41
J1834−0010	B1831−00	1.920	−0.039	0.0008(53)	49123.0	148	12.8	5.45	5.40	5.40	< −0.97	−10.98
J1834−0426	B1831−04	3.447	−0.854	0.0208(6)	50165.0	250	18.1	3.22	1.24	0.46	−1.90	−10.45
J1835−0643	B1832−06	3.270	−432.507	0.790(9)	49993.0	256	18.8	164.18	27.53	1.84	−1.37	−9.04
J1835−1106	—	6.027	−748.776	9.4(3)	51289.0	243	12.1	357.22	263.09	0.53	0.39	−8.11
J1836−0436	B1834−04	2.823	−13.239	−0.066(3)	49957.0	246	19.2	18.22	7.52	0.33	−1.67	−9.95
J1836−1008	B1834−10	1.777	−37.278	−0.024(9)	50123.0	279	17.8	37.79	36.84	0.32	−0.70	−9.04
J1837−0045	—	1.621	−4.424	−0.0033(15)	51400.0	193	11.0	1.40	1.38	1.38	< −1.52	−11.18

Table 1 – *continued*

PSR J	PSR B	ν (s^{-1})	$\dot{\nu}$ (10^{-15} s^{-2})	$\ddot{\nu}$ (10^{-24} s^{-3})	Epoch (MJD)	N	T_s (yr)	σ_1 (ms)	σ_2 (ms)	σ_3 (ms)	Δ_8	$\log \sigma_z(10\,\mathrm{yr})$
J1837−0653	B1834−06	0.525	−0.213	0.00002(17)	50014.0	242	18.9	3.10	3.10	3.10	< −1.22	−11.38
J1840+5640	B1839+56	0.605	−0.547	−0.00092(3)	49129.0	385	23.6	2.13	1.14	1.07	−1.72	−10.94
J1841+0912	B1839+09	2.622	−7.496	0.0464(13)	48854.0	374	25.3	28.65	12.80	0.50	−1.23	−9.90
J1841−0425	B1838−04	5.372	−184.443	0.024(12)	49849.0	319	18.6	22.54	21.58	0.21	−1.28	−9.82
J1842−0359	B1839−04	0.543	−0.150	0.00037(13)	49848.0	303	19.6	2.94	2.68	2.68	< −1.39	−10.92
J1844+1454	B1842+14	2.663	−13.281	0.041(8)	49766.0	388	20.3	42.12	40.40	0.40	−1.30	−9.41
J1844−0244	B1842−02	1.970	−64.936	0.073(5)	49884.0	243	19.2	36.09	25.99	2.18	−1.14	−9.52
J1844−0433	B1841−04	1.009	−3.986	−0.00111(11)	50032.0	349	18.8	1.41	1.22	0.70	< −1.86	−10.84
J1844−0538	B1841−05	3.911	−148.445	−0.066(7)	49867.0	295	19.2	20.26	17.26	0.34	−1.59	−9.83
J1845−0434	B1842−04	6.163	−143.413	0.30(4)	49610.0	211	16.7	87.29	31.31	0.71	−0.74	−9.27
J1847−0402	B1844−04	1.673	−144.702	0.0819(3)	49142.0	422	23.7	62.88	2.87	0.39	−1.40	−9.90
J1848−0123	B1845−01	1.516	−12.075	0.037(5)	50407.0	289	16.5	20.01	17.64	0.31	−1.71	−9.61
J1848−1414	—	3.358	−0.158	0.0006(19)	51269.0	142	12.0	1.12	1.12	1.12	< −1.55	−11.78
J1848−1952	B1845−19	0.232	−1.254	−0.00040(19)	50515.0	180	16.2	4.19	4.12	4.12	< −1.18	−10.78
J1849−0636	B1846−06	0.689	−21.953	−0.0109(3)	49142.0	344	23.7	16.65	5.64	0.50	−1.59	−10.16
J1850+1335	B1848+13	2.894	−12.497	−0.01152(17)	50128.0	214	18.3	1.97	0.39	0.26	< −2.11	−10.81
J1851+0418	B1848+04	3.513	−13.431	0.2067(20)	50113.0	254	18.2	29.56	4.36	1.31	< −1.22	−9.99
J1851+1259	—	0.830	−7.924	0.208(5)	50106.0	195	18.4	135.61	41.86	1.00	−1.29	−9.11
J1852+0031	B1849+00	0.459	−20.398	−0.0109(14)	49995.0	232	18.8	33.11	28.91	21.44	< −0.62	−9.50
J1852−2610	—	2.973	−0.775	0.0151(5)	51249.0	125	11.9	0.90	0.29	0.29	< −1.95	−10.78
J1854+1050	B1852+10	1.745	−1.938	0.012(5)	50869.0	266	14.2	11.43	11.30	11.30	< −0.82	−10.16
J1854−1421	B1851−14	0.872	−3.166	−0.0215(7)	50313.0	193	17.3	11.56	4.41	0.69	< −1.83	−10.06
J1856+0113	B1853+01	3.739	−2911.552	25.74(7)	50523.0	344	16.3	3040.36	145.15	1.12	−0.57	−7.56
J1857+0057	B1854+00	2.802	−0.429	−0.0040(12)	50097.0	136	18.5	2.56	2.44	2.44	< −1.18	−10.69
J1857+0212	B1855+02	2.405	−232.901	0.2459(20)	49945.0	280	18.8	72.96	8.82	0.30	−1.82	−9.58
J1857+0943	B1855+09	186.494	−0.620	−0.0015(7)	50027.0	448	18.7	0.04	0.04	0.04	< −3.41	−12.77
J1900−2600	B1857−26	1.633	−0.546	−0.00391(8)	50105.0	228	18.2	1.13	0.31	0.22	< −2.17	−11.16
J1901+0156	B1859+01	3.470	−28.379	−0.0173(20)	49345.0	133	11.6	1.05	0.83	0.27	−2.06	−10.56
J1901+0331	B1859+03	1.526	−17.359	0.091(14)	50312.0	252	17.3	55.53	50.01	0.24	−1.38	−9.24
J1901+0716	B1859+07	1.553	−5.498	0.052(16)	50016.0	365	18.9	136.35	134.19	3.26	−0.56	−8.73
J1901−0906	—	1.122	−1.032	0.00125(20)	51277.0	141	12.0	0.41	0.36	0.36	< −1.76	−11.36
J1902+0556	B1900+05	1.339	−23.098	0.0481(4)	50112.0	354	18.2	18.98	2.22	0.60	< −1.93	−10.05
J1902+0615	B1900+06	1.485	−16.990	−0.0318(7)	50300.0	403	17.2	9.25	3.36	0.36	−1.76	−10.05
J1903+0135	B1900+01	1.371	−7.582	−0.0069(6)	50430.0	243	16.6	2.95	2.21	0.15	−1.82	−10.27
J1903−0632	B1900−06	2.315	−18.223	0.267(16)	50430.0	216	16.6	62.06	40.39	0.43	−1.12	−9.29
J1904+0004	—	7.167	−6.065	0.042(5)	51269.0	147	12.0	1.79	1.40	0.44	−1.96	−10.55
J1904−1224	—	2.664	−2.634	−0.0003(7)	50695.0	147	12.3	0.62	0.62	0.62	< −1.83	−11.67
J1905+0709	B1903+07	1.543	−11.751	0.562(10)	49856.0	357	19.6	271.41	81.01	7.60	−0.35	−8.75
J1905−0056	B1902−01	1.555	−7.378	−0.0193(3)	50127.0	220	18.3	5.93	1.19	0.25	< −1.94	−10.57
J1906+0641	B1904+06	3.741	−29.895	−0.0036(3)	50016.0	247	18.9	1.02	0.78	0.30	< −2.26	−11.11
J1907+4002	B1905+39	0.809	−0.354	0.000004(97)	49144.0	382	23.7	2.44	2.44	2.44	< −1.57	−11.34
J1909+0007	B1907+00	0.983	−5.336	0.0078(10)	49121.0	329	23.6	21.56	19.41	0.47	−1.59	−9.87
J1909+0254	B1907+02	1.010	−5.634	0.0724(4)	50496.0	265	16.3	27.54	2.06	0.72	< −1.81	−9.73
J1909+1102	B1907+10	3.526	−32.811	−0.030(7)	50316.0	379	17.3	14.12	13.23	0.19	−1.62	−9.93
J1910+0358	B1907+03	0.429	−0.822	0.0305(12)	50428.0	195	16.6	32.23	15.07	4.09	< −0.86	−9.55
J1910+1231	B1907+12	0.694	−3.959	0.00079(15)	49275.0	174	22.8	2.49	2.29	2.29	<0.18	−10.90
J1910−0309	B1907−03	1.982	−8.593	−0.086(5)	50430.0	187	16.6	21.94	11.99	0.66	−1.35	−9.44
J1911−1114	—	275.805	−1.065	0.016(9)	51513.0	254	10.5	0.05	0.05	0.05	< −3.34	−13.15
J1912+2104	B1910+20	0.448	−2.042	−0.00146(12)	50299.0	253	17.2	2.18	1.72	1.72	< −1.35	−10.96
J1913+1400	B1911+13	1.918	−2.955	−0.0139(4)	50314.0	256	17.3	3.16	1.18	0.24	< −2.00	−10.64
J1913−0440	B1911−04	1.211	−5.963	0.01485(17)	47036.0	543	35.0	53.91	13.10	0.44	−1.23	−10.00
J1915+1009	B1913+10	2.472	−93.191	0.0398(12)	50389.0	455	16.8	8.22	4.06	0.29	−1.96	−10.24
J1915+1606	B1913+16	16.941	−2.476	0.0035(10)	46444.0	346	18.3	0.47	0.46	0.38	< −2.12	−11.30
J1915+1647	B1913+167	0.619	−0.155	0.00047(10)	49290.0	258	22.9	2.77	2.63	2.63	< −1.22	−10.71
J1916+0951	B1914+09	3.700	−34.482	−0.0201(8)	50312.0	291	17.3	2.65	1.43	0.24	−2.23	−10.61

Table 1 – *continued*

PSR J	PSR B	ν (s^{-1})	$\dot{\nu}$ ($10^{-15}\,s^{-2}$)	$\ddot{\nu}$ ($10^{-24}\,s^{-3}$)	Epoch (MJD)	N	T_s (yr)	σ_1 (ms)	σ_2 (ms)	σ_3 (ms)	Δ_8	$\log\sigma_z(10\,\mathrm{yr})$
J1916+1312	B1914+13	3.548	−46.005	−1.25(5)	50312.0	310	17.3	207.46	82.80	0.36	−0.20	−8.46
J1917+1353	B1915+13	5.138	−189.996	0.323(5)	50161.0	517	18.1	33.81	10.81	0.17	−2.07	−9.67
J1917+2224	B1915+22	2.348	−15.798	−0.017(6)	51813.0	208	10.3	3.80	3.63	3.63	< −1.61	−10.49
J1918+1444	B1916+14	0.847	−152.252	−0.106(8)	50088.0	476	18.5	145.13	110.76	1.04	−0.81	−9.02
J1919+0021	B1917+00	0.786	−4.739	0.0046(8)	49832.0	368	19.7	13.57	12.89	0.88	< −1.72	−10.05
J1920+2650	B1918+26	1.273	−0.056	0.0002(4)	50095.0	124	18.5	1.54	1.52	1.52	< −0.99	−11.30
J1921+1419	B1919+14	1.618	−14.657	0.0308(9)	48698.0	305	26.0	30.88	13.52	2.09	< −1.10	−10.21
J1921+1948	B1918+19	1.218	−1.329	0.0015(3)	48395.9	174	23.7	3.64	3.26	3.26	< −0.49	−10.56
J1921+2153	B1919+21	0.748	−0.754	−0.00009(3)	48469.7	304	22.1	0.50	0.48	0.48	< −2.23	−11.77
J1922+2018	B1920+20	0.853	−0.472	−0.0009(4)	50085.0	195	18.4	3.41	3.35	3.35	< −0.83	−10.61
J1922+2110	B1920+21	0.928	−7.038	0.042(3)	50305.0	344	17.3	26.56	18.98	1.10	−1.65	−9.72
J1926+0431	B1923+04	0.931	−2.130	0.0153(3)	50300.0	206	17.0	6.66	1.41	0.67	< −1.50	−10.58
J1926+1434	B1924+14	0.755	−0.125	0.00013(13)	49142.0	137	23.7	2.18	2.16	2.16	−0.72	−10.77
J1926+1648	B1924+16	1.725	−53.525	0.015(6)	50122.0	436	18.3	32.14	31.48	0.81	−1.64	−9.74
J1932+1059	B1929+10	4.415	−22.560	−0.0210(16)	46926.0	769	35.7	49.73	44.15	0.21	−1.82	−9.98
J1932+2020	B1929+20	3.728	−58.626	−0.179(4)	50302.0	224	17.2	21.32	5.38	0.26	−1.69	−9.94
J1932+2220	B1930+22	6.922	−2756.784	41.01(16)	51867.0	411	8.9	432.99	31.86	0.55	0.04	−7.96
J1933+2421	B1931+24	1.229	−12.216	0.702(13)	51014.0	580	13.7	111.46	43.12	1.03	−0.86	−8.88
J1935+1616	B1933+16	2.788	−46.642	0.01430(11)	46827.0	936	36.2	29.13	6.00	0.19	−2.31	−10.41
J1937+2544	B1935+25	4.976	−15.917	−0.0026(3)	50126.0	370	18.3	0.51	0.45	0.20	< −2.56	−11.12
J1939+2134	B1937+21	641.928	−43.314	0.0174(8)	49389.0	517	22.2	0.10	0.03	0.03	< −3.11	−12.38
J1939+2449	B1937+24	1.550	−43.898	0.72(4)	50351.0	277	13.0	122.73	76.48	1.90	−0.43	−8.52
J1941−2602	B1937−26	2.482	−5.892	−0.00815(9)	50498.0	193	16.3	1.31	0.18	0.10	< −2.17	−11.02
J1943−1237	B1940−12	1.028	−1.751	0.00039(8)	49145.0	139	23.7	1.24	1.12	0.45	< −0.90	−10.70
J1944−1750	B1941−17	1.189	−1.394	0.0095(7)	50314.0	139	17.3	4.88	3.09	1.96	< −0.98	−10.34
J1945−0040	B1942−00	0.956	−0.489	0.00008(10)	48532.0	141	27.0	1.91	1.90	1.90	< −0.46	−11.23
J1946+1805	B1944+17	2.270	−0.124	0.00035(15)	49291.0	241	22.9	0.98	0.97	0.97	< −1.75	−11.24
J1946−2913	B1943−29	1.042	−1.617	−0.00137(7)	49123.0	118	23.6	1.87	0.84	0.72	< −0.96	−11.08
J1948+3540	B1946+35	1.394	−13.723	0.0048(3)	49852.0	459	19.8	3.83	3.02	0.20	−2.30	−10.49
J1949−2524	B1946−25	1.044	−3.566	−0.00068(9)	48533.0	129	23.7	1.41	1.17	0.53	< −1.43	−10.91
J1952+1410	B1949+14	3.636	−1.694	0.0023(19)	50096.0	164	16.0	1.75	1.74	1.74	< −1.28	−11.15
J1952+3252	B1951+32	25.296	−3739.490	17.51(10)	50249.0	760	17.8	452.10	56.20	0.34	−0.57	−8.52
J1954+2923	B1952+29	2.344	−0.009	0.00002(8)	49137.0	242	16.3	0.19	0.19	0.19	< −2.16	−12.23
J1955+2908	B1953+29	163.048	−0.789	−0.002(4)	49456.0	314	21.8	0.43	0.43	0.43	−1.97	−11.89
J1955+5059	B1953+50	1.927	−5.096	−0.00908(6)	49145.0	406	23.7	4.62	0.58	0.13	< −2.59	−10.83
J1957+2831	—	3.250	−32.849	0.0180(18)	51873.0	277	10.0	1.34	1.04	0.54	−2.02	−10.60
J2002+3217	B2000+32	1.435	−216.619	−0.88(3)	50015.0	497	18.9	473.25	232.21	0.98	−0.65	−8.37
J2002+4050	B2000+40	1.105	−2.123	−0.00214(7)	50094.0	388	18.5	1.11	0.58	0.39	< −2.22	−10.95
J2004+3137	B2002+31	0.474	−16.723	−0.0111(5)	49142.0	425	23.7	28.67	18.41	0.46	< −1.59	−9.92
J2005−0020	—	0.877	−9.876	−0.002(3)	51404.0	140	11.0	3.56	3.53	3.53	< −1.30	−10.95
J2006−0807	B2003−08	1.722	−0.136	−0.0033(7)	50190.0	303	17.7	2.91	2.78	2.78	< −1.56	−10.99
J2013+3845	B2011+38	4.344	−167.035	0.0150(11)	50094.0	458	18.5	4.99	2.60	0.58	−2.13	−10.52
J2018+2839	B2016+28	1.792	−0.476	0.00469(3)	46774.0	618	36.5	12.69	1.58	0.30	< −2.43	−10.86
J2019+2425	—	254.160	−0.454	−0.032(16)	51351.0	170	11.5	0.09	0.09	0.09	< −3.08	−12.31
J2022+5154	B2021+51	1.890	−10.939	−0.0188(7)	47028.0	781	35.1	64.59	45.72	0.33	−1.95	−9.82
J2023+5037	B2022+50	2.684	−18.091	0.0403(10)	50313.0	365	17.3	7.21	3.02	0.20	< −2.28	−10.28
J2029+3744	B2027+37	0.822	−8.323	−0.0642(4)	50094.0	231	18.5	42.21	3.47	0.93	< −1.49	−9.71
J2030+2228	B2028+22	1.586	−2.225	0.0134(7)	51088.0	161	13.1	1.80	0.93	0.53	< −1.17	−10.60
J2037+3621	B2035+36	1.616	−11.771	−0.48(3)	50093.0	163	18.5	183.77	99.25	1.61	−0.75	−8.31
J2038+5319	B2036+53	0.702	−0.465	0.0012(5)	50122.0	93	13.9	1.95	1.87	1.87	< −1.00	−10.77
J2046+1540	B2044+15	0.879	−0.141	0.00006(5)	49850.0	342	19.8	0.73	0.73	0.73	< −1.98	−11.80
J2046+5708	B2045+56	2.098	−48.934	0.0100(12)	50155.0	299	18.0	5.46	4.78	1.81	< −1.49	−10.12
J2046−0421	B2043−04	0.646	−0.615	0.00018(5)	49763.0	353	20.3	0.89	0.87	0.87	< −2.05	−11.43
J2048−1616	B2045−16	0.510	−2.848	−0.00144(4)	46827.0	594	36.1	13.05	11.28	0.53	< −2.10	−10.43
J2051−0827	—	221.796	−0.626	0.011(11)	51481.0	303	10.7	0.08	0.08	0.08	−3.25	−12.80

Table 1 – *continued*

PSR J	PSR B	ν (s^{-1})	$\dot{\nu}$ ($10^{-15}\,s^{-2}$)	$\ddot{\nu}$ ($10^{-24}\,s^{-3}$)	Epoch (MJD)	N	T_s (yr)	σ_1 (ms)	σ_2 (ms)	σ_3 (ms)	Δ_8	$\log\sigma_z(10\,yr)$
J2055+2209	B2053+21	1.227	−2.017	−0.00035(8)	50095.0	254	18.5	0.54	0.51	0.51	< −1.55	−11.64
J2055+3630	B2053+36	4.515	−7.524	−0.0116(3)	49753.0	472	20.2	1.86	0.69	0.12	−2.58	−10.93
J2108+4441	B2106+44	2.410	−0.501	0.0012(3)	50315.0	292	17.3	0.64	0.61	0.61	< −1.79	−11.55
J2113+2754	B2110+27	0.831	−1.813	0.00031(4)	49133.0	384	23.6	0.89	0.79	0.71	< −1.73	−11.25
J2113+4644	B2111+46	0.986	−0.694	0.01772(8)	47007.0	601	35.2	84.39	8.20	2.56	−1.53	−10.24
J2116+1414	B2113+14	2.272	−1.494	−0.0039(4)	49855.0	373	19.8	2.25	1.87	0.41	< −2.18	−10.74
J2124+1407	B2122+13	1.441	−1.594	0.0042(3)	50276.0	79	17.2	1.54	0.73	0.73	< −0.25	−10.77
J2124−3358	—	202.794	−0.846	0.011(8)	51284.0	227	11.7	0.08	0.08	0.08	< −3.15	−12.66
J2145−0750	—	62.296	−0.115	−0.0010(4)	51173.0	470	12.3	0.02	0.02	0.02	−3.70	−13.20
J2149+6329	B2148+63	2.631	−1.177	−0.00139(11)	49852.0	388	19.8	0.67	0.56	0.23	−1.97	−10.97
J2150+5247	B2148+52	3.010	−91.574	−0.0243(11)	50094.0	401	18.5	6.18	3.68	0.20	−1.88	−10.17
J2155−3118	B2152−31	0.971	−1.169	0.0022(4)	50429.0	125	16.6	2.06	1.80	1.80	< −0.96	−11.00
J2157+4017	B2154+40	0.656	−1.477	−0.0376(4)	49686.0	474	20.5	46.24	8.26	0.98	−1.89	−9.86
J2212+2933	B2210+29	0.995	−0.491	−0.00257(14)	50093.0	304	18.5	1.75	1.18	1.12	< −1.50	−10.80
J2219+4754	B2217+47	1.857	−9.537	−0.00296(5)	46471.0	510	35.3	7.64	2.61	0.61	−1.71	−10.55
J2222+2923	—	3.554	−0.078	0.0032(15)	51671.0	258	11.0	0.97	0.95	0.95	< −2.04	−11.23
J2225+6535	B2224+65	1.465	−20.734	0.0151(11)	49142.0	517	23.7	19.39	16.46	0.80	−1.35	−9.87
J2229+2643	—	335.816	−0.171	−0.011(6)	51625.0	279	11.1	0.04	0.04	0.04	< −3.18	−13.39
J2229+6205	B2227+61	2.257	−11.489	−0.0117(9)	50081.0	215	18.2	3.88	2.80	0.45	< −1.74	−10.30
J2242+6950	B2241+69	0.601	−1.741	−0.0003(3)	50092.0	115	18.5	3.54	3.27	3.27	< −0.28	−10.72
J2248−0101	—	2.095	−2.894	0.0354(8)	51270.0	171	12.0	3.20	0.81	0.48	−1.85	−10.27
J2257+5909	B2255+58	2.716	−42.428	−0.102(3)	50502.0	236	16.1	16.41	5.88	0.14	−1.90	−9.71
J2305+3100	B2303+30	0.635	−1.165	−0.00131(11)	50302.0	278	17.4	1.44	1.14	0.70	< −1.44	−10.83
J2305+4707	B2303+46	0.938	−0.500	−0.0012(7)	50088.0	186	18.5	4.49	4.44	4.44	< −0.70	−10.70
J2308+5547	B2306+55	2.105	−0.884	−0.00551(14)	49841.0	394	19.7	2.02	0.87	0.51	< −2.12	−10.94
J2313+4253	B2310+42	2.862	−0.920	0.00629(8)	48202.7	499	26.3	3.62	0.94	0.12	−2.83	−10.99
J2317+1439	—	290.255	−0.204	−0.005(7)	51656.0	230	11.0	0.04	0.04	0.04	< −3.39	−13.19
J2317+2149	B2315+21	0.692	−0.502	−0.00008(3)	49142.0	300	20.2	0.55	0.54	0.54	< −1.85	−11.71
J2321+6024	B2319+60	0.443	−1.382	−0.00118(4)	49332.0	348	22.6	3.14	1.38	1.12	< −1.11	−10.69
J2322+2057	—	207.968	−0.418	0.007(11)	51335.0	151	11.4	0.08	0.07	0.04	< −2.99	−12.73
J2325+6316	B2323+63	0.696	−1.370	0.00053(11)	48714.0	381	26.1	4.58	4.42	4.42	< −1.16	−10.67
J2326+6113	B2324+60	4.280	−6.458	0.00202(19)	50069.0	395	18.5	0.52	0.46	0.27	−2.57	−11.29
J2330−2005	B2327−20	0.608	−1.714	−0.00007(12)	50304.0	232	17.3	1.11	1.10	1.10	< −1.37	−11.96
J2337+6151	B2334+61	2.019	−781.495	3.1256(8)	50094.0	465	18.5	1064.52	4.43	1.19	−0.33	−8.29
J2346−0609	—	0.846	−0.977	−0.0014(3)	51426.0	236	11.2	0.63	0.60	0.60	< −1.94	−11.37
J2354+6155	B2351+61	1.058	−18.219	0.0233(4)	49276.0	375	22.8	23.91	6.66	0.42	−1.89	−9.99

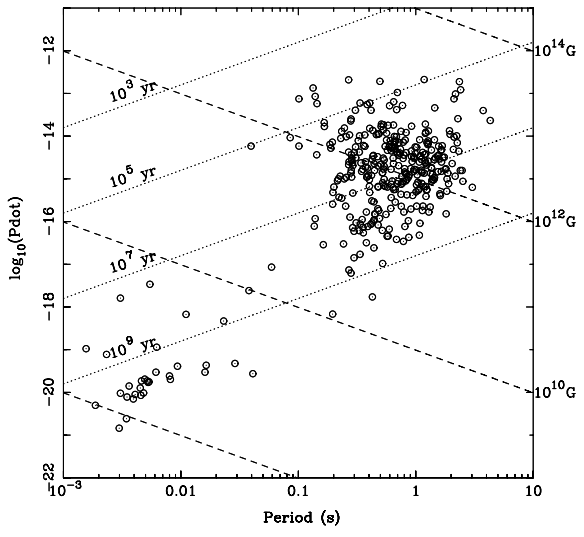

Figure 1. Period–period-derivative diagram for the pulsars in our sample.

residuals after subtracting a cubic polynomial ranges from 8 μs for PSR J1744−1134 to 460 μs for PSR B1913+16.[3] For the ordinary pulsars the rms ranges up to 948 ms for PSR B1706−16, a pulsar with a 653 ms spin period.[4]

In Fig. 3, we plot the timing residuals for all the pulsars in our sample relative to a simple slow-down model including only the pulse frequency and its first derivative. The horizontal scale of each panel represents 36 years of observations and the vertical axis is

[3] Our sample includes 31 recycled pulsars defined with spin-periods $P <$ 0.1 s and spin-down rates $\dot{P} < 10^{-17}$. We note that lower rms values have been published for some of our pulsars. For instance, Splaver et al. (2005) obtained TOA timing precisions <700 ns and as small as ∼200 ns for PSR J1713+0747 (compared with $\sim 10\mu s$ for our data). In contrast to the high-precision timing experiments that often use coherent de-dispersion systems and long observing durations, the data presented here have been obtained with a stable observing system over many years and the large sample has necessitated short observations and hence poorer TOA precision.

[4] For a large number of pulsars, the timing residuals deviate by more than one pulse period. In these cases, phase jumps of at least one period need to be added to keep track of the pulsar spin-down.

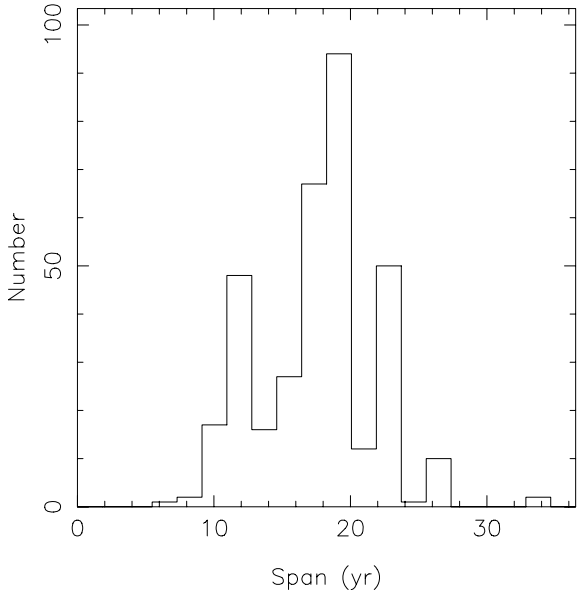

Figure 2. Histogram of the time-span of our observations.

scaled for each separate panel. The upper value gives the range from the minimum to the maximum residual in milliseconds. The lower values give the same range, but in units of the pulsars' rotational periods.

3 DISCUSSION

It is tempting to categorize the pulsars by the structures seen in their timing residuals. For instance, for approximately 37 per cent of our sample the variations in the residuals are dominated by the measurement errors caused by thermal or cosmic random noise in the observing system (e.g. PSRs B0011+47, B0045+33 and J0134−2937). 20 per cent have residuals which can be modelled by a significant positive $\ddot{\nu}$ value (such residuals take the form of a cubic polynomial), 16 per cent for a cubic polynomial corresponding to $\ddot{\nu} < 0$ and 27 per cent which show structures that are more complicated. However, this simple categorization has the following two problems.

(i) The TOAs for some pulsars are measured more precisely than for others. For instance, in Fig. 4 we plot the detailed structure observed in the timing residuals for PSR B1900+01. Any similar structure in the residuals of PSR B1745−20 (that have been overplotted in Fig. 4) would not be observable because of the much larger TOA uncertainties.

(ii) The classification of any particular pulsar is likely to change as more data are obtained. In Fig. 5, we plot the timing residuals that would have been obtained for PSR B1818−04 if we had access to data sets that spanned shorter time intervals of between 1 and 35 years. Clearly, any simple classification scheme would change depending on the length of the data span.

Glitch events lead to clear signatures in the timing residuals. As the fitting procedure used for Fig. 3 removes a quadratic term, any glitch event will exhibit a cusp (corresponding to a local maximum) in the timing residuals (good examples being PSRs B0154+61, B0525+21 and B2255+58). A large number of unpublished glitch events can be identified in these data sets and will be described in a forthcoming publication. We discuss the phenomenon known as 'slow glitches' in Section 3.2.4.

3.1 Ruling out some models of timing noise

Some pulsars in our sample are also observed as part of long-term timing programmes at other observatories. In all such cases, we see the same large-scale features and hence timing noise is not caused by observing systems or the data processing being carried out at a particular observatory. For instance, Shabanova et al. (2001) combined data from the Jodrell Bank, Hartebeesthoek and Pushchino observatories for PSR B1642−03 and saw no observatory-dependent artefacts.

The timing noise features are also not caused by the off-line processing. We have used the TEMPO2 timing package which has been designed for high-precision timing applications and is accurate for known physical effects at the 1-ns level of precision Hobbs et al. (2006). However, we have compared timing residuals using three pulsar timing packages, PSRTIME, TEMPO and TEMPO2 for many of our pulsars and see the same features in all cases. The timing procedure relies on corrections being applied to correct the observatory clocks to the terrestrial time-scale. Inaccuracies in this time transfer and in the terrestrial time-scale are expected to be at the 100 ns–1 μs level (see e.g. Rodin 2008) which will not affect the features of the timing noise described here. Finally, TEMPO2 converts the observed TOAs to barycentric arrival times using a planetary ephemeris. Changing between the DE200, DE405 and DE414 ephemerides (Standish 2004) only changes the rms timing residuals by ∼1 μs and does not affect the large-scale timing noise.

For high-precision millisecond-pulsar timing, small features in the timing residuals can occur from incomplete calibration of the polarization of the pulse profiles and are likely to be a small fraction of the pulse width. However, the timing residuals described in this paper are much larger than a typical pulse width. In addition, changes in pulse shape are likely to produce small step changes in the timing residuals. The timing noise phenomena described here produce much larger effects and have different characteristic shapes in the residuals.

It has been postulated that the effects of interstellar or interplanetary DM variations may lead to timing noise. However, any effects caused by the interstellar medium (ISM) will be dependent upon the observing frequency. As shown in Fig. 6, the timing noise seen in our data is identical at all observing frequencies and so the large-scale low-frequency noise is not caused by the ISM. It is, however, possible that some smaller scale variations are due to the ISM. A recent analysis of millisecond pulsars (You et al. 2007a) shows typical timing variations caused by variations in the pulsar's DM of up to a few microseconds (at an observing frequency ∼1.4 GHz). Interplanetary DM variations, mainly due to the solar wind (You et al. 2007b), also induce frequency-dependent residuals, but these are modelled with sufficient precision within TEMPO2.

3.2 Properties of the timing noise

3.2.1 The 'amount' of timing noise

In order to characterize the stability of each pulsar and to determine a measure of the 'amount of timing noise', we first calculate the Δ_8 value introduced by Arzoumanian et al. (1994):

$$\Delta_8 = \log_{10}\left(\frac{1}{6\nu}|\ddot{\nu}|t^3\right), \quad (1)$$

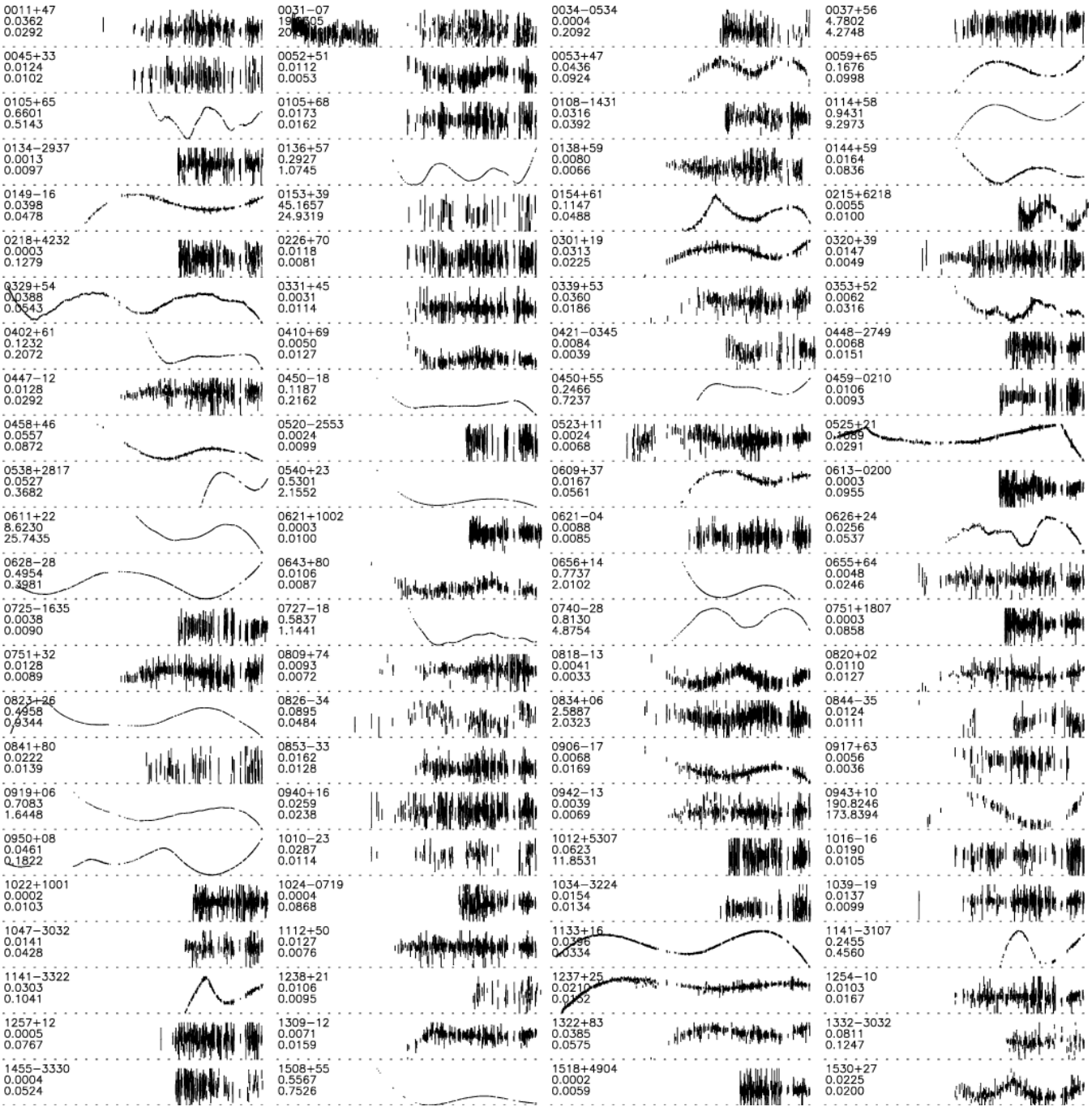

Figure 3. Timing residuals after subtraction of the pulsar's spin-frequency and its first derivative over the 38 years from MJD 39856 (year 1968) to 53736 (year 2006). The three labels on the left provide the pulsar name, the range from the minimum to maximum residuals (s) and the same range scales by the pulsar's rotational period.

where the spin-frequency, ν, and its second derivative, $\ddot{\nu}$, are measured over a $t = 10^8$ s interval.[5] As our pulsar data sets contain at least 10 yr of data, we compare the average Δ_8 value (listed in Table 1) to its variance obtained by fitting for ν and $\ddot{\nu}$ in unique 3-yr segments. Upper bounds are provided for pulsars in which the measured $\ddot{\nu}$ is not significant at the 2σ level. In Fig. 7, we plot Δ_8 versus the pulse period derivative. The dotted line corresponds to $\Delta_8 = 6.6 + 0.6 \log \dot{P}$ as obtained by Arzoumanian et al. (1994) by eye. Our data suggest that this is slightly low; a linear least-squares fit to our data for non-recycled pulsars and where the Δ_8 measurement is not an upper limit (shown as a dashed line) gives that

$$\Delta_8 = 5.1 + 0.5 \log \dot{P}. \quad (2)$$

We therefore confirm the correlation between timing noise and spin-down rate (and the implication that younger pulsars with large spin-down rates exhibit more timing noise than older pulsars) that has been described in earlier work.

[5] This interval of ∼3.16 yr has no physical meaning and was the typical data span for the Arzoumanian et al. (1994) data sets.

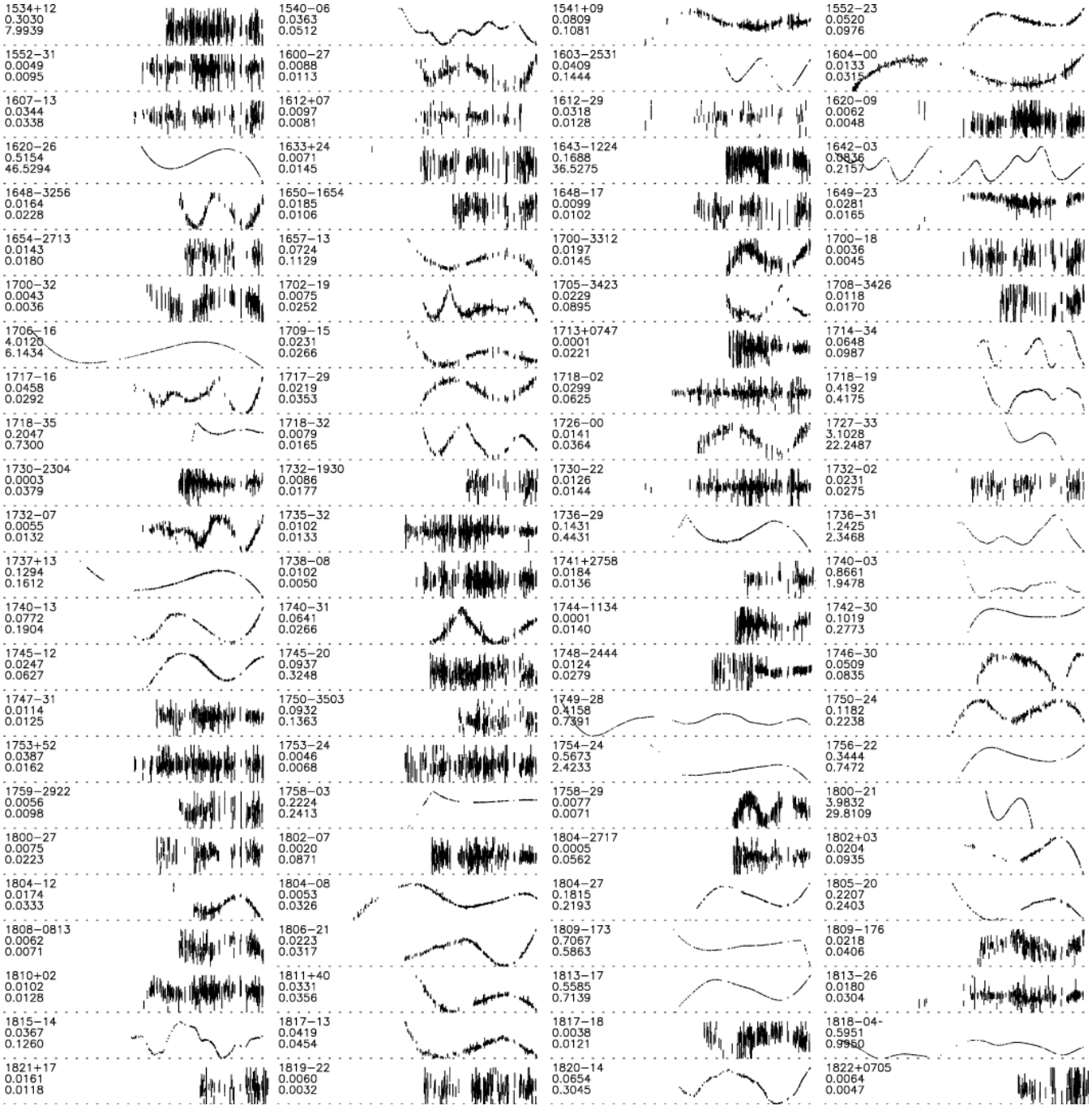

Figure 3 – *continued*

The Δ_8 parameter provides a measure of the pulsar noise at a single time-scale. Full information about the spectral components of a data set is needed to characterize the timing noise in detail. Unfortunately, both the irregular data sampling and the low-frequency noise process make power spectral determination difficult (however see Section 3.2.3). Matsakis, Taylor & Eubanks (1997) generalized the Allan variance (traditionally used for measuring clock stability) to obtain a statistic that provides a measure of pulsar stability at various time-scales. Their parameter

$$\sigma_z(\tau) = \frac{\tau^2}{2\sqrt{5}} \left\langle c^2 \right\rangle^{1/2}, \tag{3}$$

where the magnitude, c, of cubic terms fitted to short sections of the data span (of length τ) are averaged. For timing residuals whose power spectral density can be modelled as

$$S(f) \propto f^{\alpha}, \tag{4}$$

then for $\alpha < +1$, $\sigma_z(\tau)$ will also follow a power law with

$$\sigma_z(\tau) \propto \tau^{\beta}, \tag{5}$$

where $\beta = -(\alpha + 3)/2$. Models of timing noise (e.g. D'Alessandro et al. 1995) which assume that the pulsar spin is affected by a random walk in the pulse phase, frequency or slow-down rate produce a power law for the power spectral density with $\alpha = -1$, -3 and -5, respectively (corresponding to $\beta = -1, 0$ and $+1$). Timing residuals

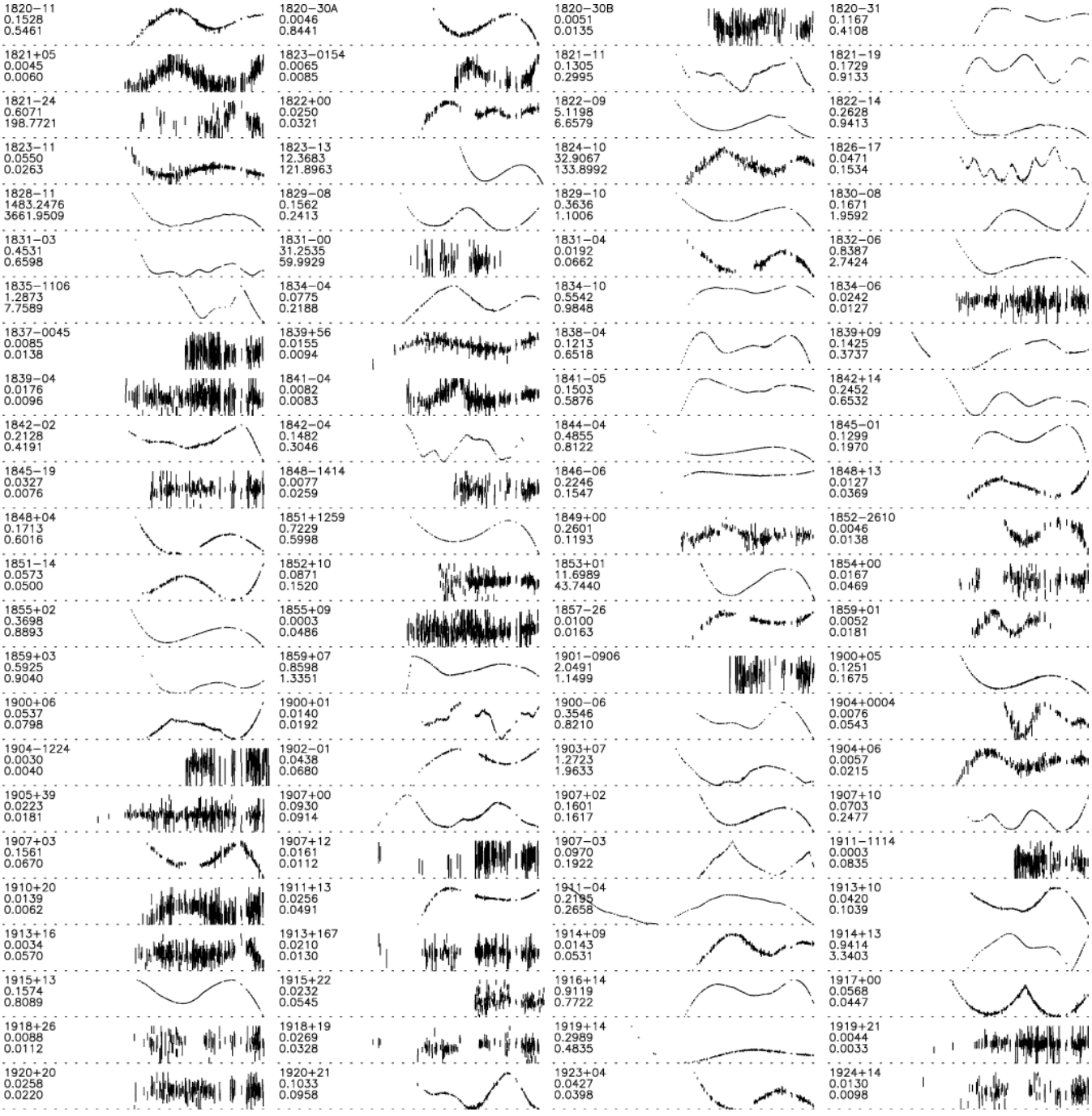

Figure 3 – *continued*

not affected by timing noise will have a flat spectrum ($\alpha = 0$) and hence $\beta = -3/2$. In Fig. 8, we show representative $\sigma_z(\tau)$ plots. As expected for PSR B0031−07, whose residuals are dominated by TOA uncertainties, $\sigma_z(\tau)$ has a gradient of $\beta = -3/2$ (dotted line) with the possibility of a turn-over corresponding to small-amplitude timing noise at large time-scales (>10 yr). The timing residuals for PSR B0628−28 were reported in D'Alessandro et al. (1995) as being consistent with phase noise ($\beta = -1$). However, our results show that $\sigma_z(\tau)$ decreases with $\beta = -1$ until a time-scale of around 2 yr before increasing with $\beta = +1$ (or $\alpha = -5$) corresponding, in the idealized model, to a random walk in $\ddot{\nu}$.$\sigma_z(\tau)$ for PSR B1642−03 has a more complex oscillatory form. We therefore confirm the conclusion of Cordes & Downs (1985) that the timing residuals cannot be modelled by a simple random walk process.

In order to search for correlations with the amount of timing noise and various pulsar parameters, we tabulate, in Table 1, $\sigma_z(10\,\mathrm{yr})$ and plot this parameter in Fig. 9. The following correlations are found.

(i) $\sigma_z(10\,\mathrm{yr})$ versus ν. The correlation coefficient measured using only the non-recycled pulsars is $\rho = 0.3$. We therefore confirm the Cordes & Helfand (1980) conclusion that timing noise is only weakly correlated with pulse period. We also highlight that the

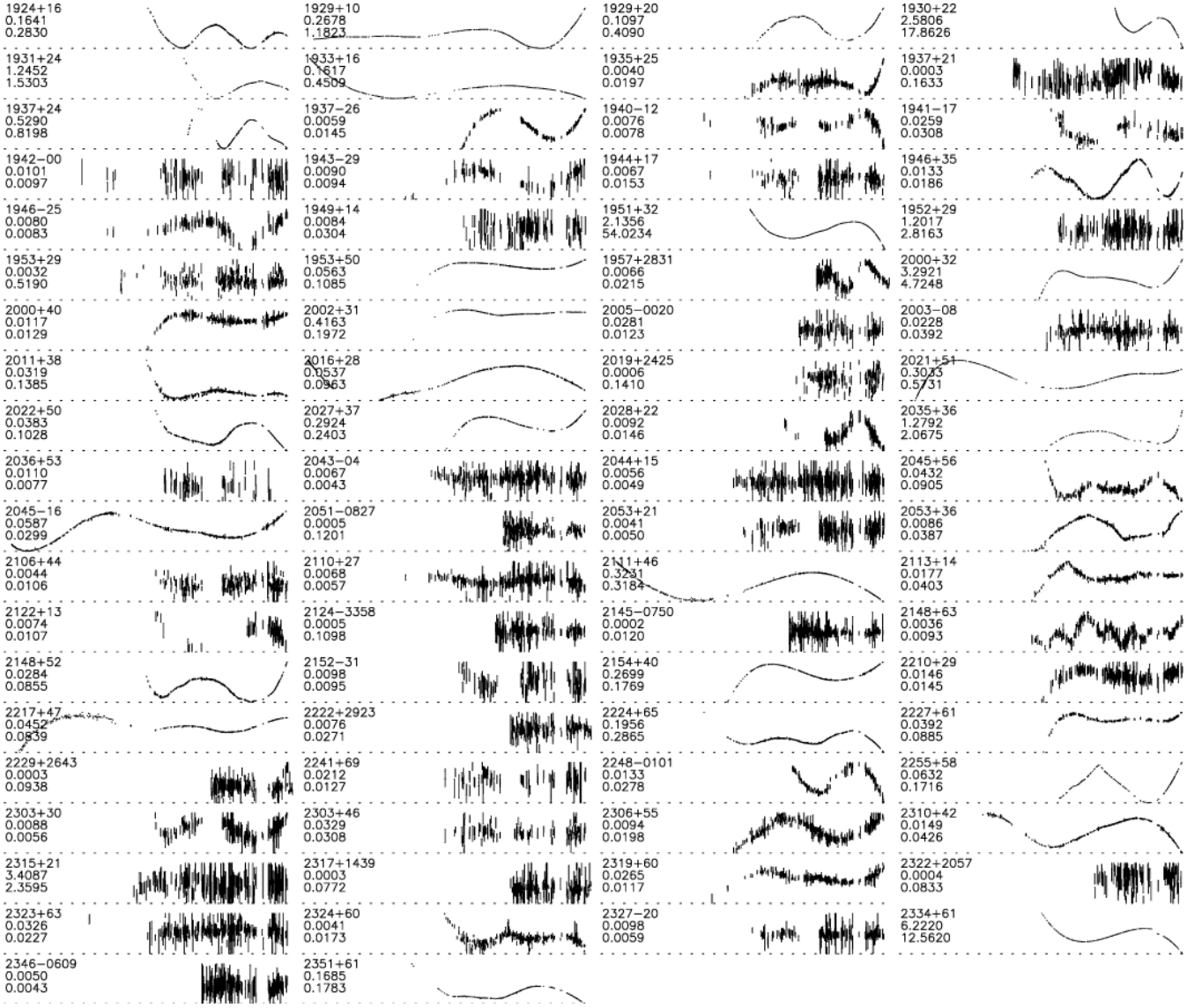

Figure 3 – *continued*

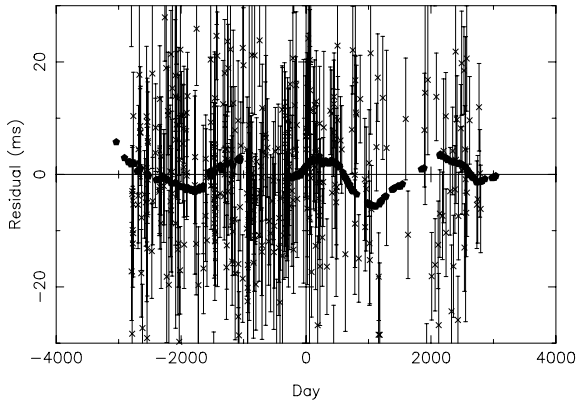

Figure 4. The timing residuals for PSR B1900+01 (filled circles) overlaid on the timing residuals for PSR B1745−20 (cross symbols).

recycled pulsars significantly deviate from the trend given by the non-recycled pulsars.

(ii) $\sigma_z(10\,\mathrm{yr})$ *versus* $\dot{\nu}$. In this case, $\rho = 0.76$ confirming that timing noise is strongly correlated with the pulse frequency derivative with pulsars having the fastest spin-down rate being more affected by timing noise than pulsars (such as the millisecond pulsars) with slower spin-down rates.

(iii) $\sigma_z(10\,\mathrm{yr})$ *versus* τ_c. The strong anticorrelation with $\dot{\nu}$ and weak correlation with ν imply that a large anticorrelation exists between timing noise and characteristic age ($\rho = -0.76$); pulsars with small characteristic ages exhibit more timing noise than older pulsars. We note that the amount of timing noise in millisecond pulsars seems to follow this correlation.

(iv) $\sigma_z(10\,\mathrm{yr})$ *versus* B_s. A weak correlation ($\rho = 0.50$) exists with the surface magnetic field strength. A significant outlying point has $B_s \sim 2 \times 10^9\,\mathrm{G}$ and corresponds to the triple pulsar system PSR B1620−26 in the globular cluster M4. The high σ_z value can be explained as being caused by the acceleration of the pulsar in the cluster's gravitational field. The timing residuals for this pulsar have

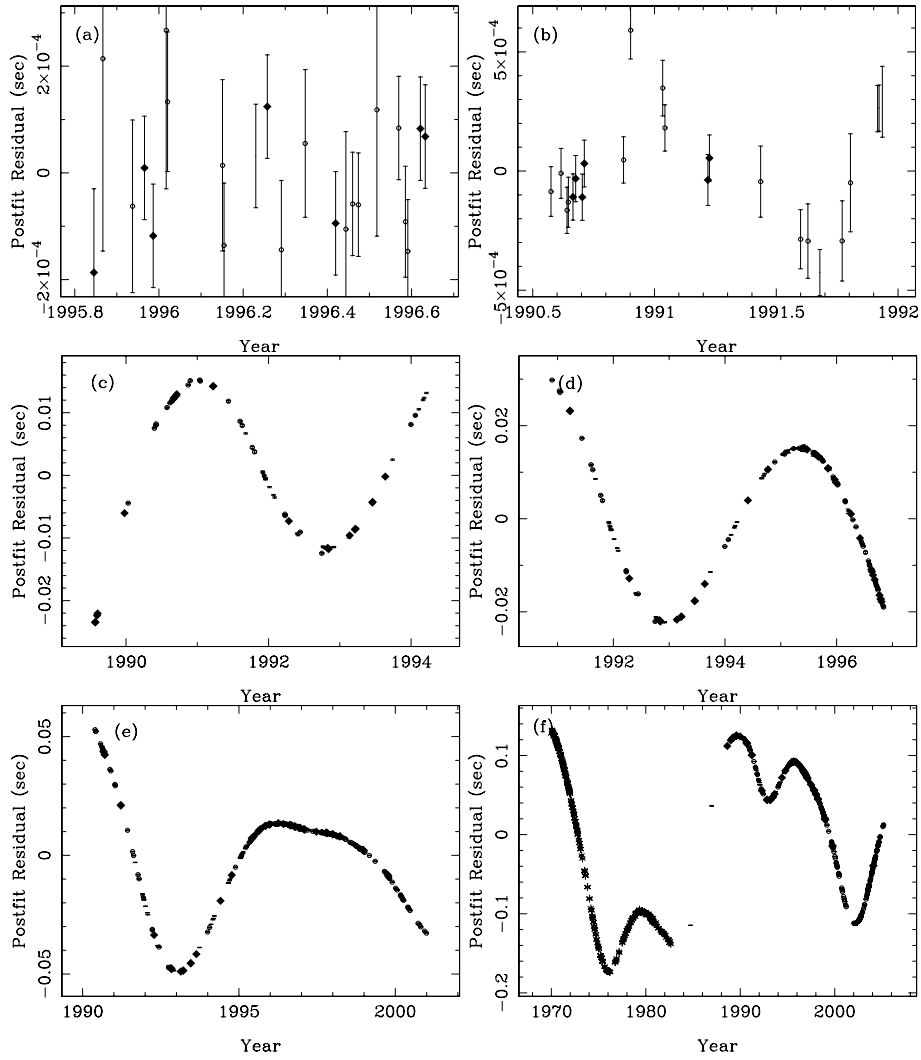

Figure 5. The timing residuals for PSR B1818−04 obtained from different section of the entire data span available. In each section, the pulsar's spin-frequency and its first derivative have been fitted. The data spans are approximately (a) 1 yr, (b) 1.5 yr, (c) 5 yr, (d) 6 yr, (e) 11 yr and (f) the full 35 years.

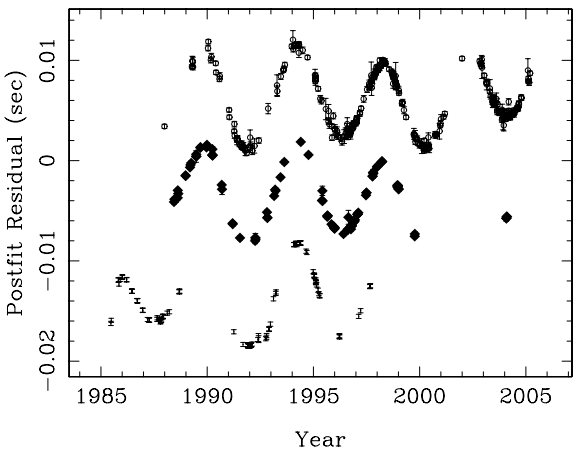

Figure 6. The timing residuals for PSR B1540−06 with an arbitrary offset applied between observations at different observing frequencies. The bottom set of residuals contains observations close to 400 MHz, the middle residuals at 600 MHz and the top at 1400 MHz.

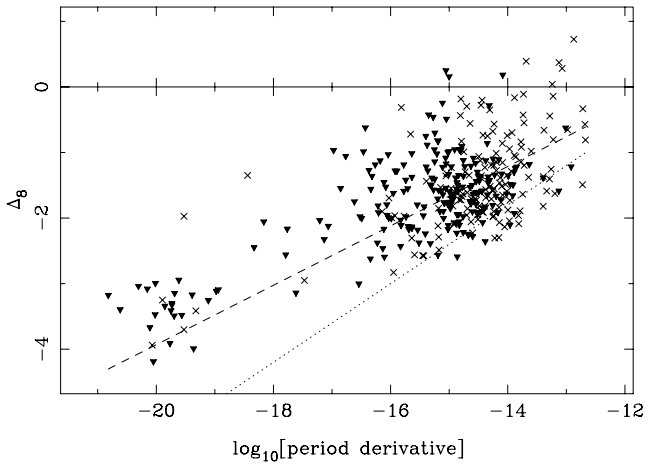

Figure 7. The Δ_8 parameter versus the pulse period derivative. Upper limits are displayed as downward pointing triangles. The dotted line gives the best fit to the data of Arzoumanian et al. (1994). The dashed line is the best-fitting straight line to our observations.

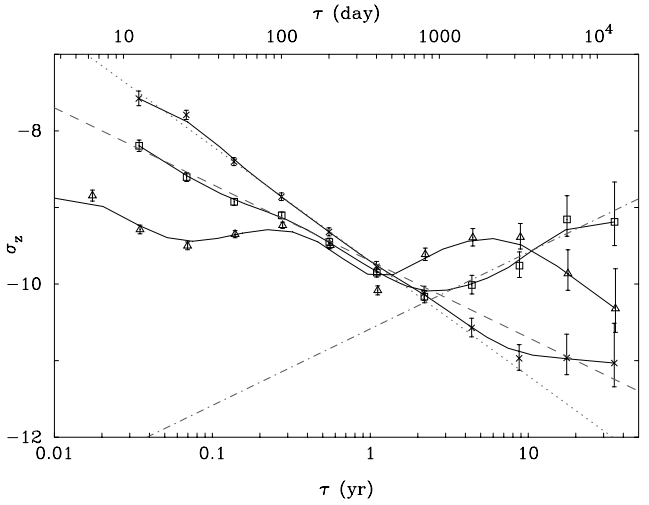

Figure 8. $\sigma_z(\tau)$ for PSRs B0031−07 (cross symbols), B0626−28 (square) and B1642−03 (triangle). The dotted line indicates timing residuals with spectral exponents of $\alpha = 0$, the dashed line for $\alpha = -1$ and the dot–dashed line for $\alpha = -5$. The solid lines are a cubic spline fit through the data points.

been studied by numerous authors (e.g. Thorsett et al. 1999; Ford et al. 2000; Beer, King & Pringle 2004).

(v) $\sigma_z(10\,\mathrm{yr})$ *versus* $\dot{E}$. A strong anticorrelation ($\rho = -0.71$) exists with the spin-down energy-loss rate $\dot{E} \propto \dot{P}/P \propto \dot{\nu}\nu$.

(vi) $\log_{10}[\sigma_z(10\,\mathrm{yr})]$ *versus* time-span. No correlation is found between the pulsar stability at 10 yr and the total observational period ($\rho = -0.03$).

In order to predict the amount of timing noise for a given pulsar, we searched through multiple combinations of $\nu^\alpha \dot{\nu}^\beta$ and obtained a maximum correlation coefficient of $\rho = 0.77$ for

$$\log_{10}[\sigma_z(10\,\mathrm{yr})] = -1.37 \log_{10}\left[\nu^{0.29}\,|\dot{\nu}|^{-0.55}\right] + 0.52. \quad (6)$$

This expression,[6] plotted in Fig. 10, allows the prediction of the amount of intrinsic timing noise over a 10 yr time-scale for any pulsar. In order for pulsar timing array experiments to be sensitive to gravitational wave signals, it is necessary for $\sigma_z(10\ \mathrm{yr}) \lesssim 10^{-14}$ (e.g. Hobbs et al. 2009). On a 10 yr time-scale, our results suggest that the residuals for the majority of the millisecond pulsars in our sample will be dominated by timing noise and not by the residuals induced by the gravitational wave background (assuming that such a background exists and that the expression above is valid for millisecond pulsars). However, there are a few pulsars where the timing noise is at a much lower level. For instance, the timing residuals for PSR J0437−4715 have an rms of ∼200 ns over a 10 yr time-scale (Verbiest et al. 2008). A study of the timing noise for the most stable millisecond pulsars is currently being undertaken and will be published elsewhere.

3.2.2 *Significant* $\ddot{\nu}$ *values*

The residuals for pulsars whose residuals are dominated by a significant $\ddot{\nu}$ value take the form of a cubic polynomial. For a pulsar slowing down by magnetic dipole braking, the value of $\ddot{\nu}$ is expected to be

$$\ddot{\nu} = \frac{n\dot{\nu}^2}{\nu}, \quad (7)$$

where the braking index, $n = 3$. The measured braking indices for the non-recycled pulsars range from −287 986 to +36 246 with a mean of −1713 and median of 22. If we restrict our sample to pulsars where we have data spanning more than 30 years, we obtain braking indices ranging from −1701 to +36 246 with a mean of +3750 and median of +29. For the simple model of magnetic dipole braking, the $\ddot{\nu}$ value will be positive. Out of our sample of 366 pulsars, 193 (53 per cent) have a positive $\ddot{\nu}$ value and the remaining 173 (47 per cent) have negative $\ddot{\nu}$ (we obtain similar statistics if we restrict our sample to only those pulsars with significantly measured $\ddot{\nu}$ values). As concluded in H04, the observed $\ddot{\nu}$ values for the majority of pulsars are not caused by magnetic dipole radiation or by any other systematic loss of rotational energy, but are dominated by the amount of timing noise present in the residuals and the data span.

Johnston & Galloway (1999, hereafter JG99) derived a new method for determining pulsar braking indices which only requires measurements of ν and $\dot{\nu}$. Our sample contains 17 pulsars that are in common with the JG99 sample. In general, our braking indices are not consistent with those in JG99. To understand the reason for this inconsistency, we consider PSR B0740−28 for which we have an ∼21 yr data span. Our measurement for n is inconsistent with JG99 who obtain a positive value $n = 25.6(8)$. With our entire data span, we obtain $n = -10.0(7)$. If we select a shorter data set between MJDs 46690 and 51162, we obtain $n = -65.7(7)$ and between MJDs 48892 and 53451 we get $n = +68.5(5)$. If we measure the pulse parameters from both the earliest 3 yr of data and the most recent, then we can use the same methodology as JG99. Using this method, we obtain that $n = 18.5(3)$. A similar analysis using ∼200 d of data gives $n = -48(2)$. The work of Alpar & Baykal (2006) was based upon JG99 and concluded that many pulsars with anomalous positive $\ddot{\nu}$ measurements obey a scaling between $\ddot{\nu}$ and glitch parameters. They also reported that negative $\ddot{\nu}$ values can be understood in terms of glitches that were missed or unresolved. However, as our results are not consistent with those analysed in the JG99 paper, the Alpar & Baykal (2006) and JG99 conclusions need to be treated with caution.

Plotting the $\ddot{\nu}$ values versus characteristic age (Fig. 11) allows us to identify that the six youngest pulsars in our sample all have $\ddot{\nu} > 0$ (as indicated with 'plus' symbols on the diagram). Glitch events prior to the first observation will induce $\ddot{\nu} > 0$ (e.g. Lyne et al. 2000). Our data are therefore consistent with the timing residuals for all pulsars younger than $\tau_c \sim 10^5$ yr being dominated by the recovery from a glitch (or from glitch events that occurred during the observation span). For the very youngest pulsars, it seems that glitch activity is small (Shemar & Lyne 1996) and any timing noise is dominated by magnetic braking. Hence, for these pulsars braking indices close to 3 are expected and observed. For pulsars with characteristic ages $>10^5$ yr, 52 per cent have $\ddot{\nu} > 0$ and the remainder (48 per cent) have $\ddot{\nu} < 0$. As almost equal numbers of pulsars have each sign of $\ddot{\nu}$, we suggest that the timing noise seen in older pulsars is not caused by glitch recovery or by magnetic braking, but from some other process.

In the timing residuals that span many years, we see many fewer cubic structures (corresponding to large, significant $\ddot{\nu}$ values) than for shorter data spans. In Fig. 12, we plot $|\ddot{\nu}|$ values obtained from the PSR B0329+59 data set with various data spans. For data spanning ∼10 yr, we measure a large, significant $\ddot{\nu}$ value and, hence, the

[6] Note that $\nu^{0.29}|\dot{\nu}|^{-0.55}$ can be written in terms of the characteristic age and pulse period as $\sim (P\tau_c)^{0.3}$.

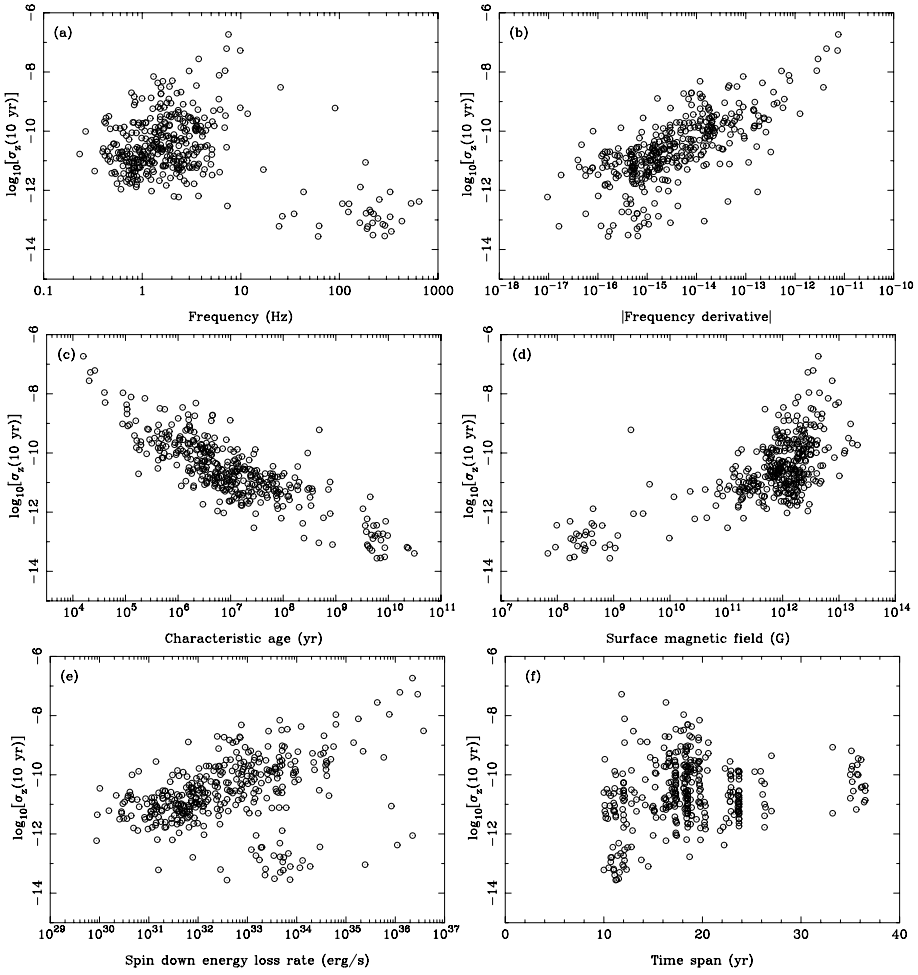

Figure 9. $\sigma_z(10\,\mathrm{yr})$ versus (a) pulse frequency, (b) frequency derivative, (c) characteristic age, (d) surface magnetic field strength, (e) energy loss rate and (f) data span.

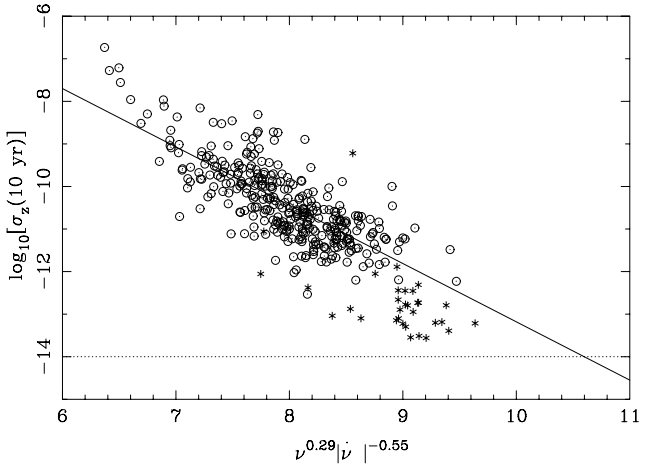

Figure 10. $\sigma_z(10\,\mathrm{yr})$ is plotted versus $\nu^{\alpha}|\dot{\nu}|^{\beta}$, where α and β were chosen to produce the highest correlation coefficient for the non-recycled pulsars (circles). The recycled pulsars are overlaid (star symbols). The horizontal dotted line is the predicted level of a gravitational wave background.

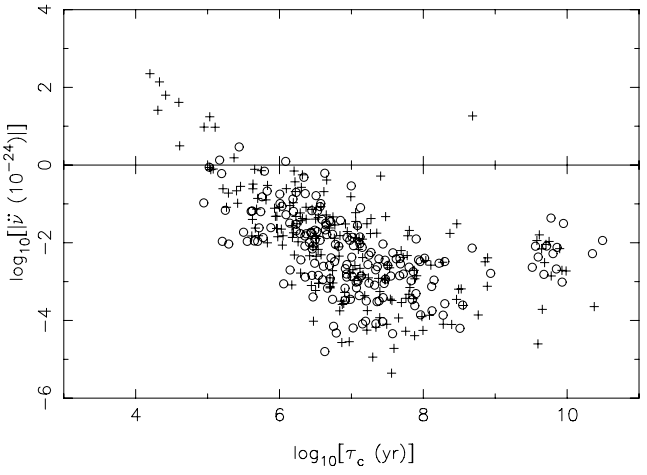

Figure 11. The measured $\ddot{\nu}$ values versus characteristic ages. Pulsars with $\ddot{\nu} > 0$ are indicated using 'plus' signs, with 'circles' for those with $\ddot{\nu} < 0$.

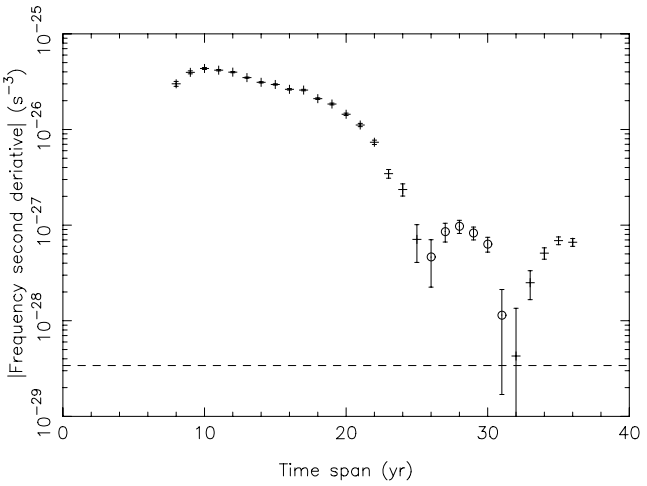

Figure 12. Values of $|\ddot{\nu}|$ obtained using differing data spans for PSR B0329+54. The circles indicate $\ddot{\nu} < 0$ and the cross symbols otherwise. The horizontal dashed line indicates $\ddot{\nu} = 3.4 \times 10^{-29}$, the value expected if the spin-down is dominated by magnetic dipole braking.

timing residuals take the form of a cubic polynomial. For data spanning more than ∼25 yr, we see no significant cubic term. The braking index measured from the $\ddot{\nu}$ value with the longest data span of $n = 75$ is still significantly greater than that expected from magnetic dipole braking.

For the pulsars dominated by a significant $\ddot{\nu}$ we plot, in Fig. 13, the timing residuals after a cubic polynomial has been fitted and removed. In the presence of a steep red-noise spectrum, we would expect the resulting residuals to be dominated by a quartic polynomial. However, in most cases we see significantly more quasi-periodic structures (good examples being PSRs B1540−06, B1826−17, B1828−11 and B1853+01). The recycled pulsars, PSR B1620−26 and B1820−30A, are unusual in that they are the only recycled pulsars with large frequency derivatives. They both lie close to the cores of globular clusters (M4 and NGC6624, respectively) and the significant $\ddot{\nu}$ values can therefore be explained as being caused by the acceleration of the pulsar in the gravitational field of the cluster as a whole or of neighbouring stars.

3.2.3 Periodicities

For each of our pulsars, we have obtained a power spectrum. A detailed description of our method for obtaining power spectra in the presence of steep red-noise and irregularly sampled data is beyond the scope of this paper and will be presented elsewhere. Here, we concentrate on those pulsars (PSRs B1540−06, B1642−03, B1818−04, B1826−17, B1828−11 and B2148+63) which show significant periodicities or quasi-periodic structures. A Lomb–Scargle power spectrum that has been oversampled by a factor of 4 (Press et al. 1986) for each of these pulsars is shown in Fig. 14 after whitening the timing residuals by fitting a $\ddot{\nu}$ term.

PSR B1540−06: A significant periodicity is observed with a period of 4.38 yr. It is possible that the periodic signal is caused by the orbital motion of an unmodelled Earth-mass planetary companion. Including such a companion in the timing fit indicates an orbital period of $P_b = 1530(3)$ d, a projected semimajor axis of $a \sin i = 0.00393(7)$ and an epoch of periastron of $T_0 = 48992(5)$. The rms timing residual decreases from 7.0 ms without subtracting a cubic term or binary companion, 3.0 ms after subtracting the cubic term alone and 1.1 ms after subtracting the cubic and binary parameters. However, significant structure remains in the timing residuals after the removal of these terms, and we do not consider this as compelling evidence for a planetary companion. In the top-left panel of Fig. 15, we show one oscillation of the timing residuals. For this pulsar, the radii of curvature (and hence the magnitude of the local value of $\dot{\nu}$) at the maxima and minima are similar.

PSR B1642−03: The timing residuals for this pulsar show a clear quasi-periodic structure. The time between successive peaks ranges from 3.4 to 6.6 yr. In Fig. 15, we show three local maxima and overplot dashed lines with a gradient of $+5 \times 10^{-5}$ s d^{-1}. We note that the radius of curvature is smaller at local maxima than minima suggesting that the residuals between a local maxima and the next minima can be modelled simply as two discrete $\dot{\nu}$ values. This pulsar therefore has three separate slow-down rates. The quasi-periodic nature of the timing residuals implies that the power spectrum (Fig. 14) does not show a single periodicity, but rather multiple low-frequency components (which we consider as evidence against the free-precession model of Shabanova et al. 2001).

PSR B1818−04: The timing residuals show a clear oscillation where the time between local maxima ranges between ∼7 and ∼10 yr. The spectrum contains significant low-frequency power, but no significant individual periodicities.

PSR B1826−17: The power spectrum for this pulsar shows a significant periodicity of 2.9 yr. However, the time between successive peaks ranges from 2.4 to 3.2 yr suggesting a variation in this periodicity of ∼10 per cent. It is clear from Fig. 15 that this pulsar is similar to PSR B1642−03 where local maxima have a smaller radii of curvature than local minima.

PSR B1828−11: The timing residuals for PSR B1828−11 are dominated by a significant frequency derivative. However, if this cubic polynomial term is fitted and removed, then the timing residuals show the clear periodic structures reported by Stairs et al. (2000). Previously, these periodicities, and correlated pulse shape changes, have been explained by free-precession of the neutron star. However, counter-theoretical arguments have been put forward stating that the interior superfluid in the neutron star would damp out any free-precessional effects on a short time-scale (Shaham 1977; Sedrakian, Wasserman & Cordes 1999). Our spectral analysis agrees with that of Stairs et al. (2000), clearly showing a highly stable significant periodicity at ∼500 d. A close-up study of one oscillation (Fig. 15) shows three components plotted as dashed lines which suggests that the local minima are made up of two components whereas local maxima only have one component.

PSR B2148+63: The timing noise is at a much lower level compared with the TOA uncertainties for this pulsar. However, the periodogram shows clear periodicities with 3.2 yr (∼1200 d), 7.1 yr and, at a lower level, 2.1 yr. In contrast to the residuals for PSR B1642−03 and B1826−17, this pulsar exhibits larger radii of curvature at local maxima than at minima.

For completeness, we note that it has often been proposed that PSR B0329+59 has planetary companions. Demiański & Prószyński (1979) and Bailes, Lyne & Shemar (1993) found a 3 yr periodicity in the timing residuals. However, Shabanova (1995) found no clear evidence for a 3-yr period, but did present the possibility of a 16.8 yr periodicity. Konacki et al. (1999) argued that

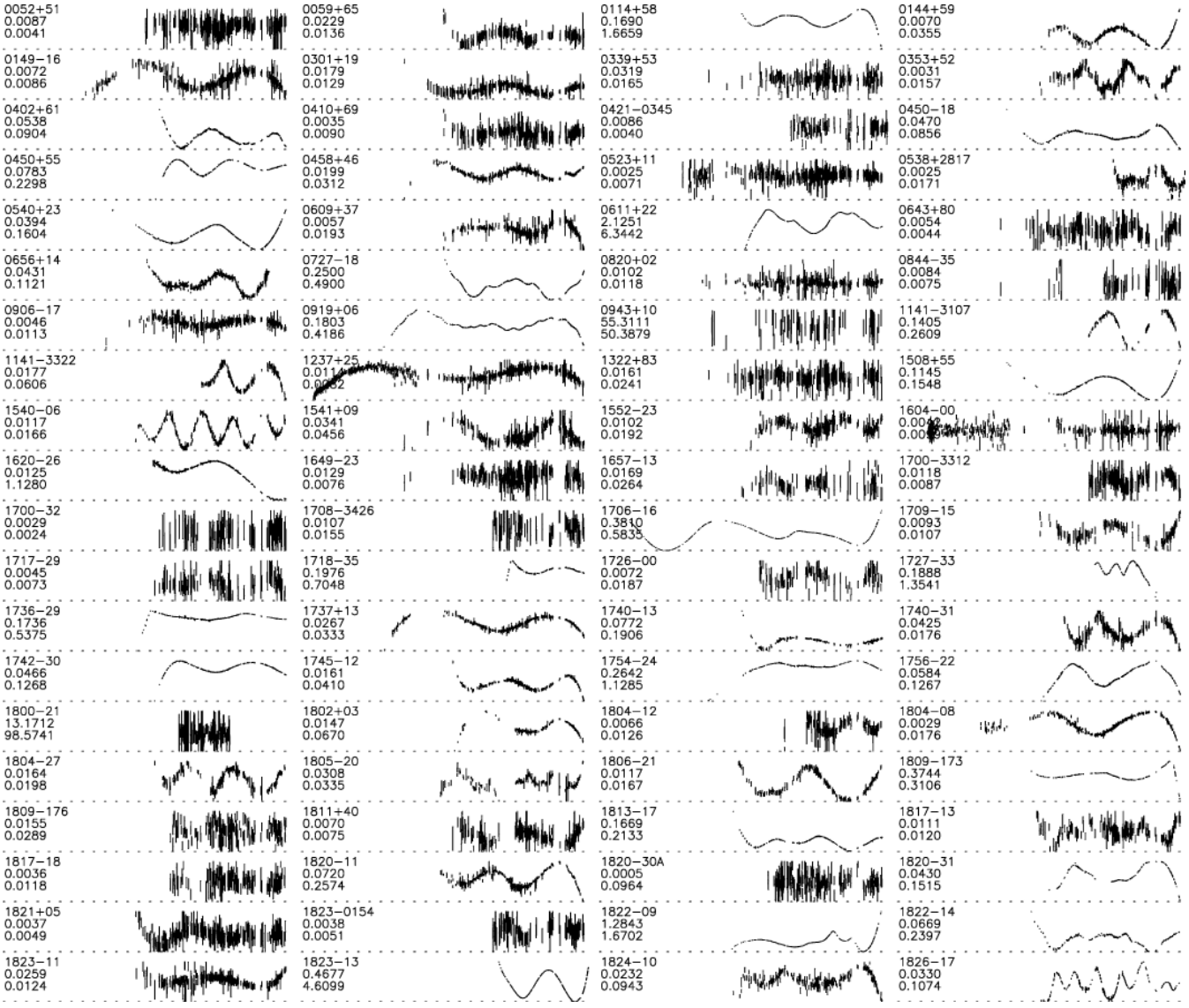

Figure 13. Pulsar timing residuals after the removal of a cubic term.

there is no evidence for planetary companions. Our data set, which spans 36.5 yr, also shows no evidence for either a 3 yr or a 16.8 yr periodicity, and we believe that the timing noise for PSR B0329+59 has a similar form to the other pulsars in our sample.

3.2.4 Slow glitches

Zou et al. (2004) reported a phenomenon known as 'slow glitches' for PSRs B1822−09 and J1825−0935. 'Slow glitches' are characterized by a permanent increase in frequency, but no significant change in the slow-down rate. More recently, Shabanova (2007) identified a further five slow glitches in the timing of PSR B1822−09. In Fig. 16, we present our timing residuals for this pulsar between MJD 49708 and 53426. The epochs of the slow glitches reported by Shabanova (2007) are indicated by vertical lines. The observed timing residuals are not dissimilar to those plotted in Fig. 15 and described in Section 3.2.3. We therefore suggest that slow glitches are not a unique phenomenon, but are caused by the same process as the timing noise seen in our sample of pulsars.

4 CONCLUSION

We have presented the timing residuals of 366 pulsars over the past 36 years. These residuals show the following.

(i) Timing noise is widespread in pulsars (Section 2).

(ii) The timing noise described here is not an artefact of the observing systems or offline processing (Section 3.1).

(iii) Timing noise is inversely correlated with characteristic age, τ_c (Section 3.2.1).

(iv) The timing noise cannot be explained using a simple random walk model in the pulse phase, frequency or spin-down rate (Section 3.2.1).

(v) The structures seen in the timing noise vary with data span. As more data are collected, more quasi-periodic features are observed.

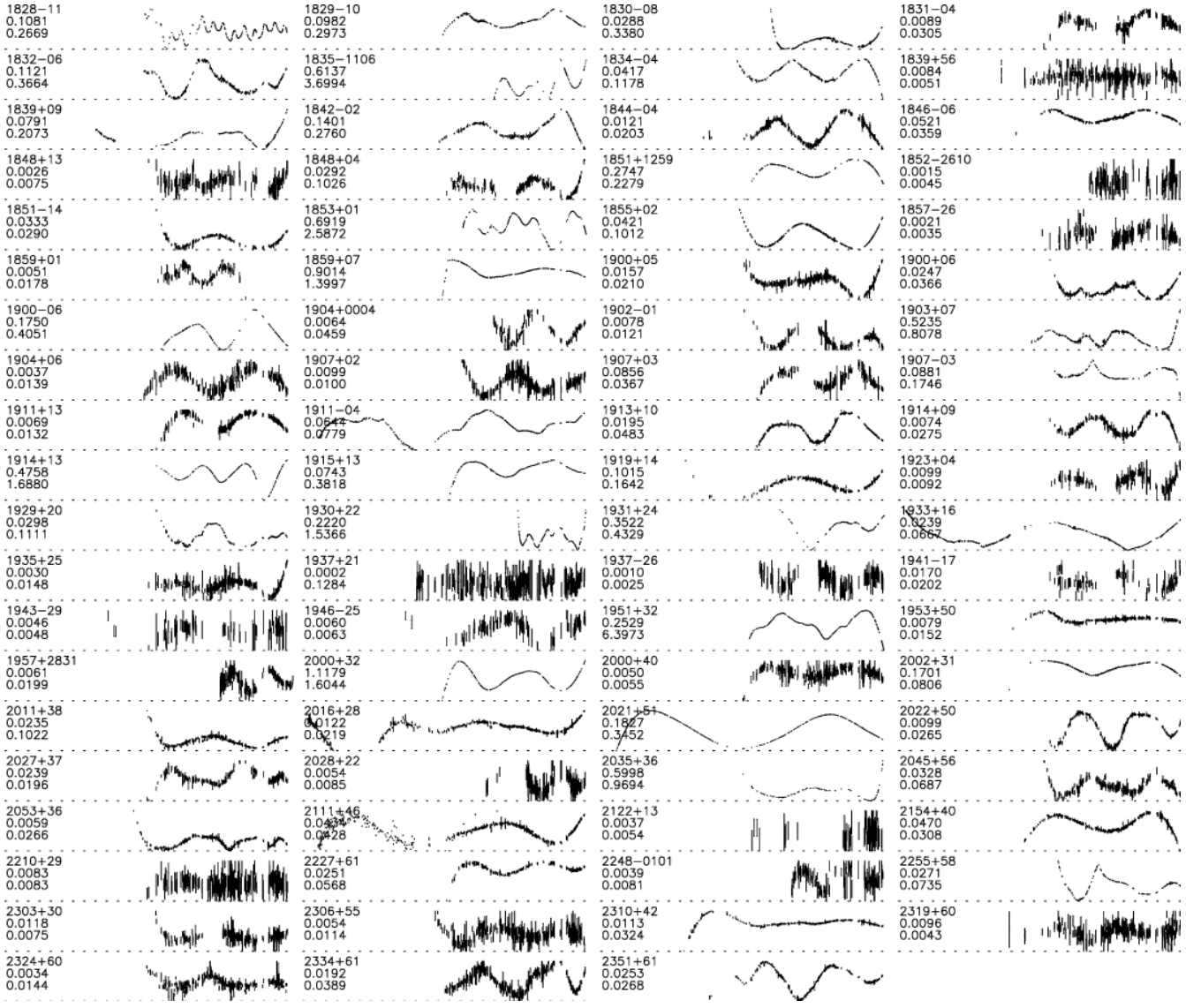

Figure 13 – *continued*

Shorter data spans generally exhibit a significant $\ddot{\nu}$ term that is not related to the magnetic braking of the neutron star (Section 3.2.2).

(vi) The dominant contribution to timing noise for all pulsars with $\tau_c < 10^5$ can be explained as being caused by the recovery from previous glitch events (Section 3.2.2).

(vii) Significant periodicities are seen in the timing residuals of a few pulsars (e.g. PSRs B1540−06, B1826−17, B1828−11 and B2148+63). However, quasi-periodic structures are seen in the timing residuals of many pulsars (Section 3.2.3).

(viii) The detailed structure of the timing noise indicates that local maxima usually have different radii of curvature than local minima (Section 3.2.3).

(ix) There is no evidence for a planetary companion to PSR B0329+54 (Section 3.2.3).

(x) 'Slow glitches' are not likely to be a different phenomenon to that causing timing noise (Section 3.2.4).

We emphasize that these results could only have been found by studying the timing residuals over very long data spans and further work is continuing to search for correlated pulse shape changes and to relate the glitch phenomena with timing noise.

ACKNOWLEDGMENTS

During the course of this work, we made extensive use of NASA's Astrophysics Data System bibliographic data base and the astro-ph preprint service. GH is the recipient of an Australian Research Council QEII Fellowship (DP0878388). Many people have been involved in timing pulsars from Jodrell Bank Observatory. In particular, we acknowledge Christine Jordan and the many telescope operators who have overseen the thousands of observations used in this paper.

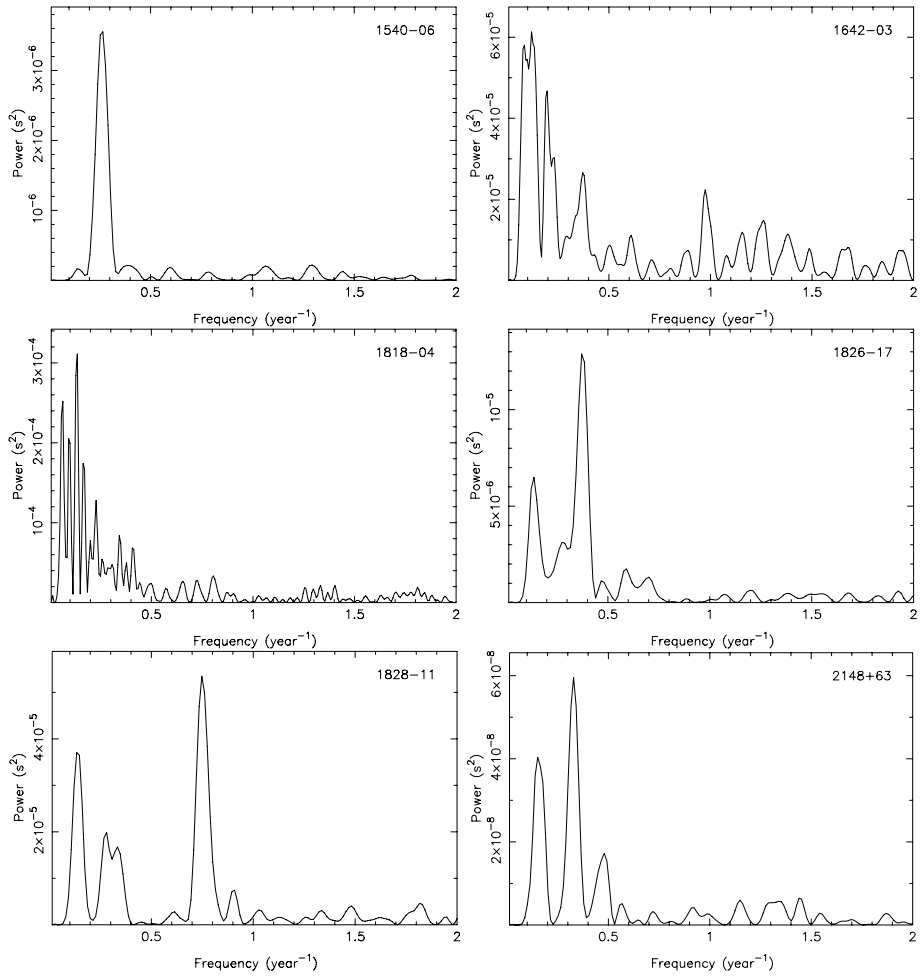

Figure 14. Power spectra of PSRs B1540−06, B1642−03, B1818−04, B1826−17, B1828−11 and B2148+63.

REFERENCES

Alpar M. A., Baykal A., 2006, MNRAS, 372, 489

Arzoumanian Z., Nice D. J., Taylor J. H., Thorsett S. E., 1994, ApJ, 422, 671

Bailes M., Lyne A. G., Shemar S. L., 1993, in Phillips J. A., Thorsett S. E., Kulkarni S. R., eds, ASP Conf. Ser. Vol. 36, Planets Around Pulsars. Astron. Soc. Pac., San Francisco, p. 19

Baykal A., Ali Alpar M., Boynton P., Deeter J., 1999, MNRAS, 306, 207

Beer M. E., King A. R., Pringle J. E., 2004, MNRAS, 355, 1244

Boynton P. E., Groth E. J., Hutchinson D. P., Nanos G. P., Partridge R. B., Wilkinson D. T., 1972, ApJ, 175, 217

Cordes J. M., 1993, in Phillips J. A., Thorsett S. E., Kulkarni S. R., eds, Planets around Pulsars. Astron. Soc. Pac. Conf. Ser., Vol. 36, p. 43

Cordes J. M., Downs G. S., 1985, ApJS, 59, 343

Cordes J. M., Helfand D. J., 1980, ApJ, 239, 640

D'Alessandro F., McCulloch P. M., Hamilton P. A., Deshpande A. A., 1995, MNRAS, 277, 1033

Demiański M., Prószyński M., 1979, Nat, 282, 383

Downs G. S., Krause-Polstorff J., 1986, ApJS, 62, 81

Downs G. S., Reichley P. E., 1983, ApJS, 53, 169

Edwards R. T., Hobbs G. B., Manchester R. N., 2006, MNRAS, 372, 1549

Ford E. B., Joshi K. J., Rasio F. A., Zbarsky B., 2000, ApJ, 528, 336

Hobbs G., 2005, Proc. Astron. Soc. Australia, 22, 179

Hobbs G. et al., 2002, MNRAS, 333, L7

Hobbs G., Lyne A. G., Kramer M., Martin C. E., Jordan C., 2004, MNRAS, 353, 1311 (H04)

Hobbs G., Lorimer D. R., Lyne A. G., Kramer M., 2005, MNRAS, 360, 974

Hobbs G. B., Edwards R. T., Manchester R. N., 2006, MNRAS, 369, 655

Hobbs G. et al., 2009, Proc. Astron. Soc. Australia, 26, 103

Janssen G., Stappers B., 2006, A&A, 457, 611

Johnston S., Galloway D., 1999, MNRAS, 306, L50 (JG99)

Konacki M., Lewandowski W., Wolszczan A., Doroshenko O., Kramer M., 1999, ApJ, 519, L81

Livingstone M. A., Kaspi V. M., Gavriil F. P., Manchester R. N., 2005, ApJ, 619, 1046

Lorimer D. R., Kramer M., 2005, Handbook of Pulsar Astronomy. Cambridge Univ. Press, Cambridge

Lyne A., 2009, in Arzoumanian Z., Van der Hooft F., van den Heuvel E. P. J., eds, Pulsar Timing, General Relativity and the Internal Structure of Neutron Stars. Edita KNAW, Amsterdam, p. 141

Lyne A. G., Smith F. G., 2004, Pulsar Astronomy, 3rd edn. Cambridge Univ. Press, Cambridge

Lyne A. G., Shemar S. L., Graham-Smith F., 2000, MNRAS, 315, 534

Manchester R. N., Taylor J. H., 1977, Pulsars. Freeman, San Francisco

Matsakis D. N., Taylor J. H., Eubanks T. M., 1997, AA, 326, 924

Melatos A., Peralta C., Wyithe J. S. B., 2008, ApJ, 672, 1103

Press W. H., Flannery B. P., Teukolsky S. A., Vetterling W. T., 1986, Numerical Recipes: The Art of Scientific Computing. Cambridge Univ. Press, Cambridge

Rodin A. E., 2008, MNRAS, 387, 1583

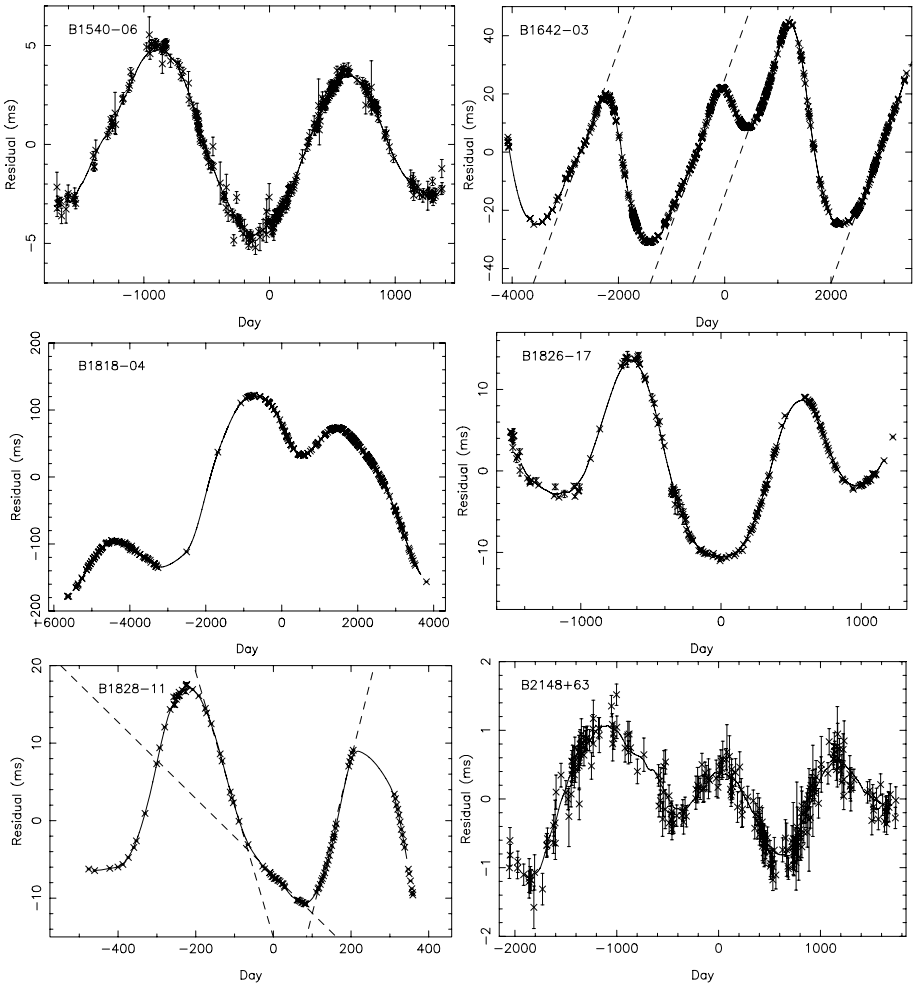

Figure 15. Short sections of the timing residuals for PSRs B1540−06, B1642−03, B1818−04, B1826−17, B1828−11 and B2148+63. A smoothed, constrained cubic spline curve is plotted through the data points.

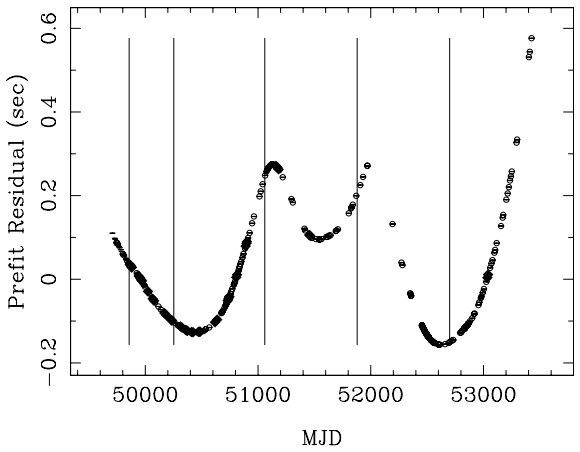

Figure 16. The timing residuals for PSR B1822−09 from MJD 49708 to 53426. The time of 'slow-glitch' events as reported by Shabanova (2007) is indicated by vertical lines.

Sedrakian A., Wasserman I., Cordes J. M., 1999, ApJ, 524, 341
Shabanova T. V., 1995, ApJ, 453, 779
Shabanova T. V., 2007, Ap&SS, 308, 591
Shabanova T. V., Lyne A. G., Urama J. O., 2001, ApJ, 552, 321
Shaham J., 1977, ApJ, 214, 251
Shemar S., Lyne A. G., 1996, MNRAS, 282, 677
Splaver E. M., Nice D. J., Stairs I. H., Lommen A. N., Backer D. C., 2005, ApJ, 620, 405
Stairs I. H., Lyne A. G., Shemar S., 2000, Nat, 406, 484
Standish E. M., 2004, AA, 417, 1165
Thorsett S. E., Arzoumanian Z., Camilo F., Lyne A. G., 1999, ApJ, 523, 763
Verbiest J. P. W. et al., 2008, ApJ, 679, 675
Warszawski L., Melatos A., 2008, MNRAS, 390, 175
You X. P., Hobbs G. B., Coles W. A., Manchester R. N., Han J. L., 2007a, ApJ, 671, 907
You X. P., Hobbs G. B., Coles W. A., Manchester R. N., Han J. L., 2007b, ApJ, 671, 907
Zou W. Z., Wang N., Wang H. X., Manchester R. N., Wu X. J., Zhang J., 2004, MNRAS, 354, 811

This paper has been typeset from a TEX/LATEX file prepared by the author.